# Cobalt(II) Pentaaza-Macrocyclic Schiff Base Complex as Catalyst for Light-Driven Hydrogen Evolution in Water: Electrochemical Generation and Theoretical Investigation of the One-Electron Reduced Species

Robin Gueret, Carmen Castillo, Mateusz Rebarz, Fabrice Thomas, Michel Sliwa, Jérôme Chauvin, Baptiste Dautreppe, Jacques Pécaut, Jérôme Fortage, Marie-Noëlle Collomb

# A Cobalt(II) Pentaaza-Macrocyclic Schiff Base Complex as Catalyst for Light-Driven Hydrogen Evolution in Water: Electrochemical Generation and Theoretical Investigation of the One-Electron Reduced Species

Robin Gueret,[†] Carmen E. Castillo,[†] Mateusz Rebarz,[‡,∥] Fabrice Thomas,*[,†] Michel Sliwa,[‡] Jérôme Chauvin,[†] Baptiste Dautreppe,[†,§] Jacques Pécaut,[§] Jérôme Fortage,*[,†] and Marie-Noëlle Collomb*[,†]

[†] Univ. Grenoble Alpes, CNRS, DCM, 38000 Grenoble, France

[‡] Université de Lille, CNRS, UMR 8516, LASIR, Laboratoire de Spectrochimie Infrarouge et Raman, F59 000 Lille, France

[§] Univ. Grenoble Alpes, CEA, CNRS, INAC-SyMMES 38000 Grenoble, France

**KEYWORDS:** Cobalt, photocatalysis, hydrogen, homogeneous catalysis, DFT.

**ABSTRACT**.

We previously reported that the tetraazamacrocyclic Schiff base complex $[Co^{III}(CR14)(X)_2]^{n+}$ (CR14 = 2,12-dimethyl-3,7,11,17-tetraazabicyclo[11.3.1]heptadeca-1(17),2,11,13,15-pentaene, X = Cl (n = 1) (**1**-$Cl_2$) or $H_2O$ (n = 3) (**1**-$(H_2O)_2$)) is a very efficient $H_2$-evolving catalyst (HEC) in fully aqueous solutions at pH 4.0 – 4.5 when used in a photocatalytic system including a photosensitizer and ascorbate as sacrificial electron donor. The excellent $H_2$-evolving activity of this complex, compared to other cobalt and rhodium catalysts studied in the same photocatalytic conditions, can be related to the high stability of its two-electron reduced form, the putative "Co(I)" state. These very interesting results led us to investigate the $H_2$-evolving performances of a series of compounds from a close-related family, the pentaazamacrocyclic cobalt $[Co^{II}(CR15)(H_2O)_2]Cl_2$ complex (**2**, CR15 = 2,13-dimethyl-3,6,9,12,18-pentaazabicyclo[12.3.1]octadeca-1(18),2,12,14,16-pentaene), which comprises a larger macrocycle with five nitrogen atoms instead of four. Electrochemical as well as spectroscopic investigations in $CH_3CN$ coupled to density functional theory (DFT) calculations point to decoordination of one of the amine upon reduction of Co(II) to the low-valent "Co(I)" form. The resulting unchelated amine could potentially act as a proton relay promoting the $H_2$ formation via proton-coupled-electron transfer (PCET) reactions. Besides, the iron, manganese and zinc analogues, $[Fe^{II}(CR15)(X)_2]^{n+}$ (X = Cl (n = 0) or $H_2O$ (n = 2)) (**3**), $[Mn^{II}(CR15)(CH_3CN)_2](PF_6)_2$ (**4**) $\{[Zn^{II}(CR15)Cl](PF_6)\}_n$ (**5**) were also synthetized and investigated. The photocatalytic activity of **2**-**5** toward protons reduction was then evaluated in a tri-component system containing the $[Ru^{II}(bpy)_3]Cl_2$ photosensitizer and ascorbate, in fully aqueous solution. The photocatalytic activity of **2** was also compared with that of **1** in the same experimental conditions. It was found that the number of catalytic cycle *versus* catalyst for **2** are slightly lower than that of **1**, suggesting that if the amine released upon reduction of **2** plays a role in promoting the $H_2$-evolving catalytic activity, other factors balance this effect. Finally, photophysical and nanosecond transient absorption spectroscopy were used to investigate the photocatalytic system.

## INTRODUCTION

Hydrogen ($H_2$) is considered as one of the energy carriers of the future, which represents a very interesting alternative to fossil fuels. Within this frame, $H_2$ need to be produced by a "sustainable" approach such as water-splitting using solar energy, mimicking photosynthesis in plants.[1] A large number of artificial photosynthesis systems that promote the reduction of water (or protons) into $H_2$, the reduction part of the water-splitting reaction, rely on molecular photocatalytic systems in homogeneous solution that typically associate a $H_2$-evolving catalyst, a photosensitizer to absorb visible light and a sacrificial electron donor which supplies the required electrons. Many efforts have been done to develop efficient molecular $H_2$-evolving catalysts based on such three-component photocatalytic systems. However, due to their poor stability/solubility in water, studies are generally performed in organic or mixed organic:aqueous solvents. While the pioneering studies in fully aqueous solution employed molecular catalysts based on Rh[2] and Pt,[3] efficient photocatalytic systems using more earth-abundant metal ions (*i. e.* Co,[4] Fe,[5] and Ni[6]) have emerged in 2012, demonstrating that even non precious metal based catalysts can be performant in water.[7] Most of the studies are related to cobalt complexes with polypyridyl ligands[4a, 7-8]. Some of them achieve very high turnover numbers (TONs) versus catalyst when a high ratio of photosensitizer/catalyst is used, in association with a very low catalyst concentration (< 1 μM). Among the cobalt systems active in water, we reported the tetraazamacrocyclic Schiff base complex $[Co^{III}(CR14)(X)_2]^{n+}$ (CR14 = 2,12-dimethyl-3,7,11,17-tetraazabicyclo[11.3.1]heptadeca-1(17),2,11,13,15-pentaene, X = Cl (n = 1) (**1**-$Cl_2$) or X = $H_2O$ (n = 3), (**1**-$(H_2O)_2$)) (Scheme 1). This complex exhibits a high catalytic activity at pH 4.0 when associated to either a molecular photosensitizer ($[Ru^{II}(bpy)_3]Cl_2$ (**Ru**) or triazatriangulenium organic dye)[9] or semiconductor nanocrystals quantum dots (CdTe or $CuInS_2/ZnS$).[10] In all of these systems, water was buffered with ascorbate and ascorbic acid ($HA^-/H_2A$), which act as the electrons and protons source, respectively. Interestingly, systematic comparative studies conducted by our group in the same experimental conditions have shown that the $H_2$-evolving activity of **1** when used in a photocatalytic system with **Ru** as photosensitizer in acidic water (pH ~ 4) exceeds significantly that of several other rhodium and cobalt catalysts. Indeed, the amount of $H_2$ produced (TONs vs catalyst) by **1** is higher than that of $[Rh^{III}(dmbpy)_2Cl_2]^+$ (dmbpy = 4,4'-dimethyl-2,2'-bipyridine)[11] and much higher than the derivatives, $[Rh^{III}(bpy)Cp^*(H_2O)]SO_4$ ($Cp^*$ = $\eta^5$-$C_5Me_5$),[11a] $[Co^{III}(N4Py)(H_2O)]^{3+}$ (N4Py tetrapyridyl N5 ligand),[12] $[Co^{III}\{(DO)(DOH)pn\}Br_2]$,[13]

$[Co(dmbpy)_3]^{2+}$,[9a] and finally the Wilkinson catalyst $Na_3[Rh^I(dpm)_3Cl]$ (dpm = diphenylphosphinobenzene-m-sulfonate).[11a] Besides, a recent systematic comparative photocatalytic study by the group of Artero[14] also reveals that, overall, the $H_2$-evolving catalytic activity of this compound in water at pH 4.5 far exceeds that of several other family of molecular catalysts such as cobaloximes,[13, 15] nickel thiolate,[16] diiron carbonyl[17] and platinum complexes.[18]

**Scheme 1. Photosensitizer (Ru) and Catalysts (1-5) Studied in this Work**.

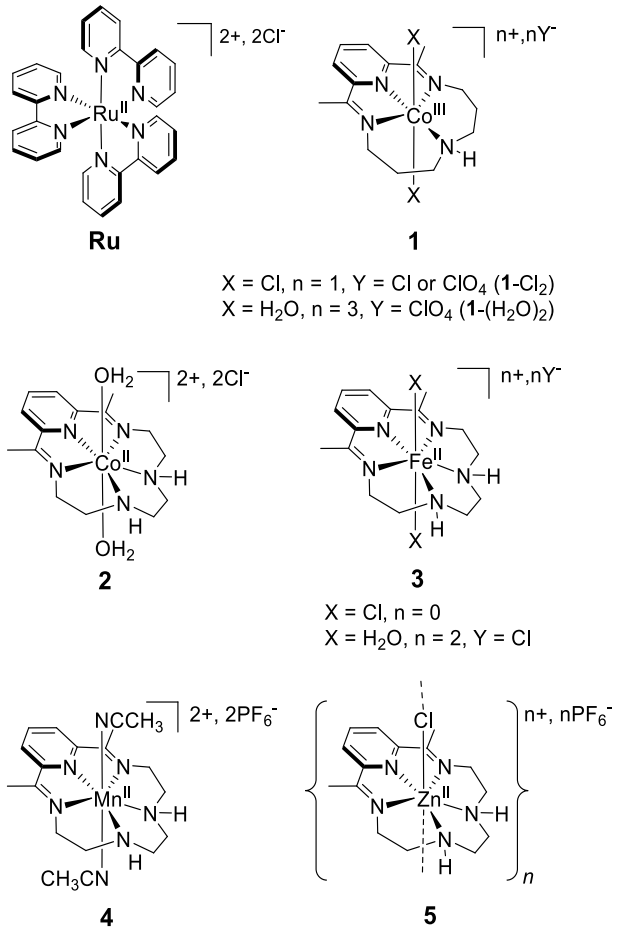


The high catalytic performance of the $[Co^{III}(CR14)(X)_2]^{n+}$ complex (**1**) can be related to the high stability of its two-electron reduced form, the formally "Co(I)" state (metal or ligand-centered reduction process), as well as its reactivity towards protons. The stability of this low-valent species, fully consistent with the macrocyclic nature of the CR14 ligand, has been established by its electrochemical generation in $CH_3CN$[9a, 9b] and its chemical isolation.[19] Stability in neutral solutions and reactivity towards protons of the reduced form of a $H_2$-evolving catalyst are key

points for the catalytic performances. Indeed, the common mechanism of $H_2$ production proposed is the protonation of the "Co(I)" species to form the Co(III) hydride intermediate (denoted Co(III)-H).[9a, 9b, 20] Nevertheless, recent studies point out the involvement of unusual ligand-centered protonation events in hydrogen evolution catalysis and related proton-coupled-electron-transfer (PCET) reactions, which appear in some cases to occur in place of hydride formation or at least form structures that are in equilibrium with the more traditional metal hydrides.[21]

The excellent $H_2$-evolving activity of **1** in a photocatalytic system with **Ru** as photosensitizer[9a] prompts us to investigate the performance toward $H_2$ production of a series of compounds from a close-related family. In this work, we evaluate for the first time the activity of the heptacoordinated pentaazamacrocyclic cobalt $[Co^{II}(CR15)(H_2O)_2]Cl_2$ complex (**2**, CR15 = 2,13-dimethyl-3,6,9,12,18-pentaazabicyclo[12.3.1]octadeca-1(18),2,12,14,16-pentaene), which comprises a larger macrocycle with five nitrogen atoms instead of four (Scheme 1). Since low-valent "Co(I)" species prefer tetra- or pentacoordinated geometry,[9b, 19a, 22] the decoordination of one of the amine is expected upon reduction of this Co(II) complex into "Co(I)". We envision that this non-coordinated amine in close proximity to the metal center at "Co(I)" state could act as a proton relay for fostering $H_2$ production by PCET reactions.[13, 23] Following this reasoning, we investigated in this article the nature of the "Co(I)" state of **2** through its electrochemical generation in $CH_3CN$ as well as its *in situ* characterization by UV-visible absorption and $^1H$ NMR spectroscopies. The electronic structure of **2**, under its initial and one-electron reduced form was also evaluated by density functional theory (DFT). Besides, the iron, manganese and zinc analogues, $[Fe^{II}(CR15)(X)_2]^{n+}$ (X = Cl (n = 0) or $H_2O$ (n = 2)) (**3**), $[Mn^{II}(CR15)(CH_3CN)_2](PF_6)_2$ (**4**) $\{[Zn^{II}(CR15)Cl](PF_6)\}_n$ (**5**) were synthetized and investigated. Note that the cobalt and iron derivatives have been recently reported to be active catalysts for $CO_2$ reduction.[24] Herein, the photocatalytic activity of **2-5** toward water reduction was evaluated in fully aqueous solution within a conventional tri-components system containing the **Ru** photosensitizer and the $HA^-/H_2A$ acid couple. The catalytic activity of **2** was also compared with that of **1** in the same experimental conditions in order to establish if the introduction of an additional amine improves the $H_2$-evolving catalytic activity. Finally, an exhaustive photophysical study was carried out in order to identify the initial steps of the photocatalytic cycle for the **Ru**/**2**/$HA^-/H_2A$ system.

## RESULTS AND DISCUSSION

**Synthesis and Crystal Structures of the Complexes.** The synthetic procedure towards compounds **2-5** was inspired from that described previously for **1** by Busch.[25] It relies on a Schiff base condensation of 2,6-diacetylpyridine with triethylenetetramine in presence of the appropriate metal ion (see Experimental Section) which acts as template. For the iron complex, the synthesis was performed in anaerobic conditions in order to avoid the oxidation of Fe(II) into Fe(III). Metallic complexes with the CR15 ligand have already been published, notably with cobalt, iron, and manganese as well as with other metals.[26] The crystal structures of $[Co^{II}(CR15)(H_2O)_2]Cl_2$ (**2**),[27] $[Mn^{II}(CR15)(H_2O)_2](PF_6)_2$,[28] and $[Fe^{II}(CR15)(H_2O)_2]Cl_2$,[29] were previously reported. We obtained a similar structure for the cobalt complex upon crystallization in water, while the crystallization of the manganese derivative in acetonitrile led to $[Mn^{II}(CR15)(CH_3CN)_2](PF_6)_2$ (**4**) in which the aquo axial ligands have been substituted by acetonitrile (see Figure S1, Tables S1 and S2). Complexes **2** and **4** exhibit a distorted pentagonal bipyramid geometry in which the metal is heptacoordinated to two aquo or acetonitrile ligands in apical position and five nitrogen atoms of the CR15 ligand that are almost co-planar with the metal. Regarding the iron derivative **3**, the poor quality of the crystals obtained has prevented the resolution of the structure. Nevertheless, according to elemental analysis and mass spectrometry (see Experimental Section), the $Fe^{2+}$ ion should be coordinated by two axial aquo or chloro molecules and, in the equatorial plane, by the five nitrogen atoms of the CR15 ligand, leading to a similar pentagonal bipyramid geometry to that of the iron(III) analogue $[Fe^{III}(CR15)(H_2O)_2]Cl_2$ already reported.[29] Single-crystals of the new zinc derivative, **5**, have been successfully obtained. Complex **5** displays a linear polymeric structure, $\{[Zn^{II}(CR15)Cl](PF_6)\}_n$ in which the $Zn^{2+}$ ions are linked to each other via chloride ligands (Figure S1 and Table S1-S2) resulting also in a heptacoordinated metallic center. According to mass spectrometry (see Experimental Section), the polymeric structure dissociates in solution leading to a six-coordinate zinc ion with only one chloride remaining coordinated in apical position.

**Electrochemical Properties of 2-5 in $CH_3CN$.** The redox properties of **2-5** were investigated in acetonitrile (Figures 1-3 and Table S3). The cyclic voltammogram (CV) of the cobalt complex **2** in $CH_3CN$, 0.1 M $[Bu_4N]ClO_4$ displays three one-electron processes. If the more positive one is clearly a metal-centered process, Co(III)/Co(II) ($Ep_a$ = +0.43 V; $Ep_c$ = -0.17 V vs $Ag/AgNO_3$), the two quasi-reversible reduction processes, formally assigned to "Co(II)/Co(I)" ($E_{1/2}$ = -1.20 V ($Ep_c$

= -1.31 V; $Ep_a$ = -1.10 V) and "Co(I)/Co(0)" ($E_{1/2}$ = -1.87 V) can be either metal or ligand centered reduction as the pyridyldiimine moiety of the ligand can be potentially reduced twice (Figure 1A).[9b, 30] An additional irreversible one-electron process is also observed at $Ep_a$ = +0.84 V that matches with the oxidation of chloride anions.[31] According to the intensity of the wave, only one of the two chloro counter-anions of **2** is present in solution, indicating that the other one coordinates the metal center to form $[Co^{II}(CR15)(CH_3CN)Cl]^+$. These observations are consistent with the strong shift of the metal-centered oxidation process Co(II)/Co(III) towards more positive potentials, after the chloro ligands have been removed from the medium by using $NaCF_3SO_3$ as supporting electrolyte (Figure 2A). In such electrolyte, the chloride anions indeed precipitate as insoluble NaCl.[31] It is worth noting that the lower electron-donating properties of $CH_3CN$ compared to the $Cl^-$ anion, for the *in-situ* generated $[Co^{II}(CR15)(CH_3CN)_2]^{2+}$ complex, results in a shift of the oxidation wave to $Ep_a$ = +1.32 V. The associated Co(III) into Co(II) appears at $Ep_c$ = +0.13 V. By contrast, the potentials of the reduction waves, "Co(II)/Co(I)" and "Co(I)/Co(0)" (Figures 1A and 2A) are not much affected by the presence or not of a chloro ligand, indicating that the chloro ligand, if coordinated, is released upon the reduction process of Co(II) into "Co(I)".

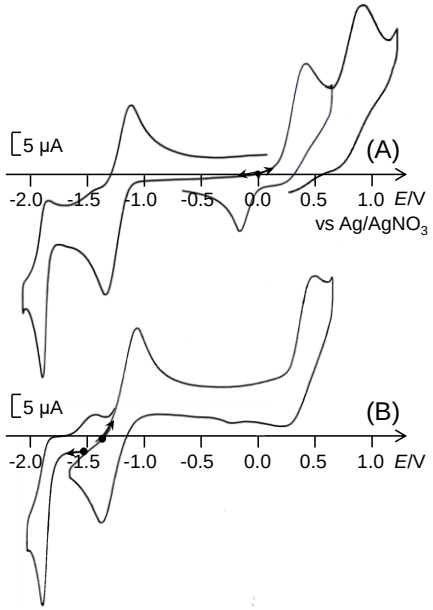


**Figure 1.** Cyclic voltammograms at a glassy carbon electrode ($\nu$ = 100 mV $s^{-1}$) of 1 mM solution of $[Co(CR15)(H_2O)_2]Cl_2$ (**2**) in $CH_3CN$, 0.1 M $[Bu_4N]ClO_4$ (A), and after an exhaustive reduction at -1.44 V vs $Ag/AgNO_3$ leading to the formation of the "Co(I)" species (B).

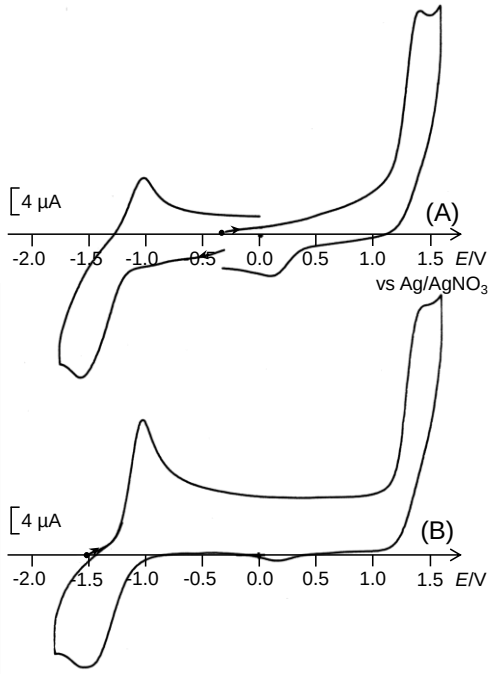


**Figure 2.** Cyclic voltammograms at a glassy carbon electrode ($\nu$ = 100 mV $s^{-1}$) of 1 mM solution of $[Co(CR15)(H_2O)_2]Cl_2$ (**2**) in $CD_3CN$, 0.1 M $NaCF_3SO_3$ (A), and after an exhaustive reduction at -1.50 V vs $Ag/AgNO_3$ leading to the formation of the "Co(I)" species (B).

The redox potentials of the reduction waves of **2** are shifted to more negative values with respect to the cobalt CR14 derivative **1**, by ~ 340-400 mV for "Co(II)/Co(I)" (for **1**-$(H_2O)_2$ and **1**-$Cl_2$, $E_{1/2}$ = -0.79 and -0.86 V, respectively) and ~ 80 mV for "Co(I)/Co(0)" ($E_{1/2}$ = -1.79 V for **1**-$(H_2O)_2$ and **1**-$Cl_2$) (Table S3).[9a] This substantial shift for the "Co(II)/Co(I)" wave is consistent with the electron-donating effect of the extra amine coordinated to the metal center which enhances the electron density on the metal center. The cyclic voltammograms of the iron and manganese complexes, **3** and **4**, exhibit one reversible M(III)/M(II) oxidation process ($E_{1/2}$ = -0.53 V (**3**) and $E_{1/2}$ = +0.84 V (**4**)) as well as two successive quasi-reversible processes assigned to the mono- and bi-reduced states of the ligand (for CR15/$CR15^{\bullet-}$, $E_{1/2}$ = -1.65 V (**3**) and -1.58 V (**4**); for $CR15^{\bullet-}$/$CR15^{2-}$, $E_{1/2}$ = -1.87 V (**3**) and -1.82 V (**4**)) (Figure 3 and Table S3). In the case of **3**, the two choride anions coordinate to the metal center which makes it much more oxidizable than the parent manganese complex, **4** (M(III)/M(II) more positive by about +1.4 V). In fact, no oxidation process is observed in the positive potential window, which attests the absence of free chloride ions in solution.[31] In the case of the zinc derivative **5**, only the ligand centered redox processes are observed at $Ep_c$ = -1.66 V and $E_{1/2}$ = -1.85 V, the Zn ion being redox inactive (Figure 3C). Since the reduced "Co(I)" form of **2** plays a pivotal role in $H_2$ evolution catalysis, its stability was

investigated by bulk electrolysis at -1.44 V in $CH_3CN$, 0.1 M $[Bu_4N]ClO_4$ (or -1.50 V in $CD_3CN$, 0.1 M $NaCF_3SO_3$). This species is quantitatively formed after exchange of one electron per molecule of initial complex, as shown by the resulting cyclic voltammograms (Figures 1B and 2B). The resulting green solutions are very stable (several days under inert atmosphere) and present identical absorptions spectra in both electrolytes ($CH_3CN$, 0.1 M $[Bu_4N]ClO_4$ or $CD_3CN$, 0.1 M $NaCF_3SO_3$) (Figure 4, spectra (c, d)). Such excellent stability was also previously observed in the case of **1** and was ascribed to the macrocyclic nature of the CR14 ligand.[9a, 12]

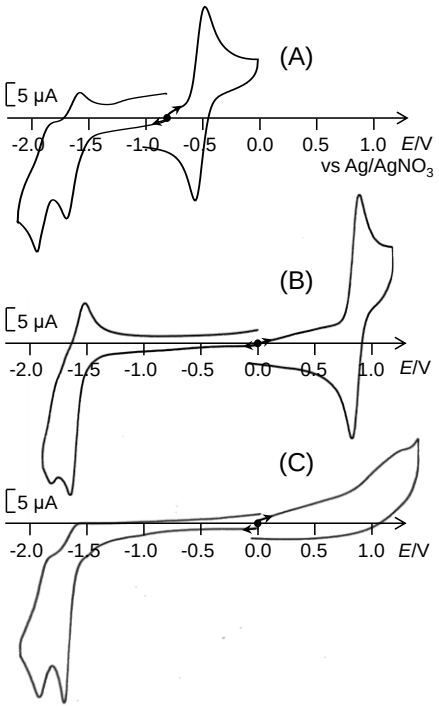


**Figure 3.** Cyclic voltammograms at a glassy carbon electrode ($\nu$ = 100 mV $s^{-1}$) of 1 mM solutions of $[Fe(CR15)Cl_2]$ (**3**) (A), $[Mn(CR15)(CH_3CN)_2](PF_6)_2$ (**4**) (B) and $\{[Zn(CR15)Cl](PF_6)\}_n$ (**5**) (C) in $CH_3CN$, 0.1 M $[Bu_4N]ClO_4$.

Besides, the similarity of the absorption spectra of the one-electron reduced form of **2** in the presence or absence of chloride, with two intense transitions at 341 and 454 nm associated with a large absorption centered at 698 nm, suggests an identical coordination sphere and thus that no chloride anion remains coordinated to the metal center in the low valent "Co(I)" state of **2**. These spectra also mirror that of the "Co(I)" species of **1** (Figure 4, spectrum (e)), revealing a close coordination sphere, *i.e.* a square pyramidal geometry involving an apical ligand (*i.e.* $CH_3CN$ or $H_2O$)[19] or eventually a square planar geometry without apical ligand,[9b] as previously proposed for

**1**. These results strongly support the release of one secondary amine of the CR15 ligand upon reduction of **2**, resulting in a "Co(I)" state only coordinated by four nitrogen atoms (Scheme 2).

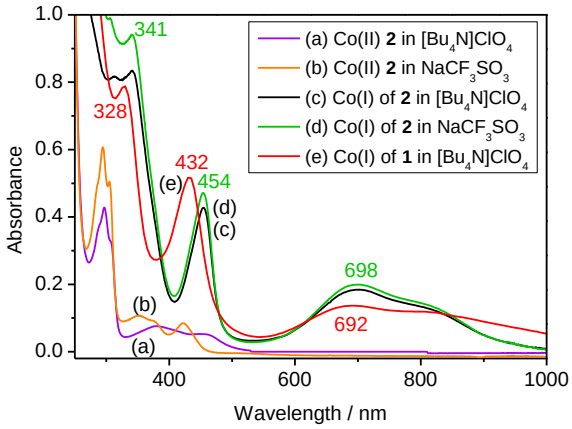


**Figure 4.** UV-visible absorption spectra of 1 mM solution of **2** in $CH_3CN$, 0.1 M $[Bu_4N]ClO_4$ (a) and in $CD_3CN$, 0.1 M $NaCF_3SO_3$ (b), after formation of Co(I) by an exhaustive reduction at -1.44 V in $CH_3CN$, 0.1 M $[Bu_4N]ClO_4$ (c) and at -1.50 V in $CD_3CN$, 0.1 M $NaCF_3SO_3$ (d), and of the Co(I) form of $[Co(CR14)(H_2O)_2](ClO_4)_3$ (**1**) obtained by a two-electron exhaustive reduction at -1.10 V of a 1 mM solution of **1** (e). Optical pathlength 1 mm.

**Scheme 2. Proposed Change in Geometry of 2 Induced by the First Reduction Process in $CH_3CN$.**

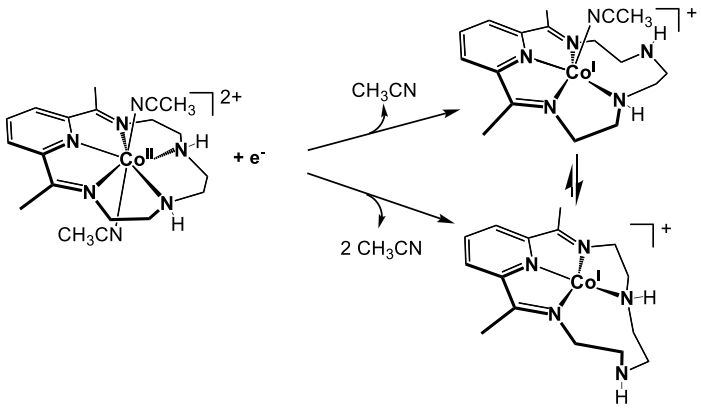


The great stability of the "Co(I)" solutions has made possible further investigation of the structure of this species by nuclear magnetic resonance ($^1$H NMR) in $CD_3CN$, 0.1 M $NaCF_3SO_3$. The release of the amine at the "Co(I)" state is observed indirectly on the NMR spectrum of the electrogenerated solution by a splitting of some aliphatic peaks (*i.e.* $CH_2$) at 2.9 and 2.8 ppm, integrating for one proton instead of two induced by the inherent dissymmetrization of the CR15

ligand (Figure S2). The splitting of $CH_2$ peaks is not observed in the $^1H$ NMR spectrum of the zinc derivative **5** as the CR15 ligand remains almost planar and penta-coordinated to the metal within a $C_S$ symmetry (Figure S3). This decoordination process upon reduction of **2** is also supported by DFT calculations (*vide supra*).

**DFT Investigations on the Cobalt Complex (2) under its Reduced Form.** The bis(imino)pyridine ligand has been previously proposed to support a rich redox chemistry once engaged in coordination.[32] The one-electron reduced complex denoted $\mathbf{2}^+$ may be therefore formulated as either a Co(I) or a Co(II)-anion radical species. In order to gain deeper insight into the reliability of both electronic structures we undertook DFT calculations.

We first optimized geometries in which the cobalt is seven-coordinate with two axially bound acetonitrile molecules (Complex **A** in Figure 5), six- (Complex **B** in Figure 5) and five-coordinate (Complex **C** in Figure 5) with one apical acetonitrile ligand, as well as four-coordinate (Complex **D** in Figure 5). We considered three spin states, the quintet $^5\mathbf{2}^+$, the triplet $^3\mathbf{2}^+$ and the closed-shell singlet $^1\mathbf{2}^+$, as well as the broken symmetry (BS) (1,1) and (1,3) solutions. The quintet state arises from a ferromagnetic interaction between the high-spin Co(II) center and an anionic ligand radical. It could be converged for both **A** and **B**, wherein the metal lies in a pentagonal bipyramidal or pentagonal pyramidal geometry. The triplet corresponds to a low spin Co(II) ion ferromagnetically exchange-coupled to a ligand radical, while the closed-shell singlet is a genuine Co(I) complex. For these two spin states, the optimized structures showing four- and five-coordinate metal center could be readily converged (**C** and **D**, respectively). In both cases one amine is uncoordinated, with a $Co\text{-}N_{amine}$ bond distance *trans* to the pyridine >4 Å). As a consequence the metal ion environment in **C** and **D** is close to that reported for $\mathbf{1}^+$ (Scheme 1).[33]

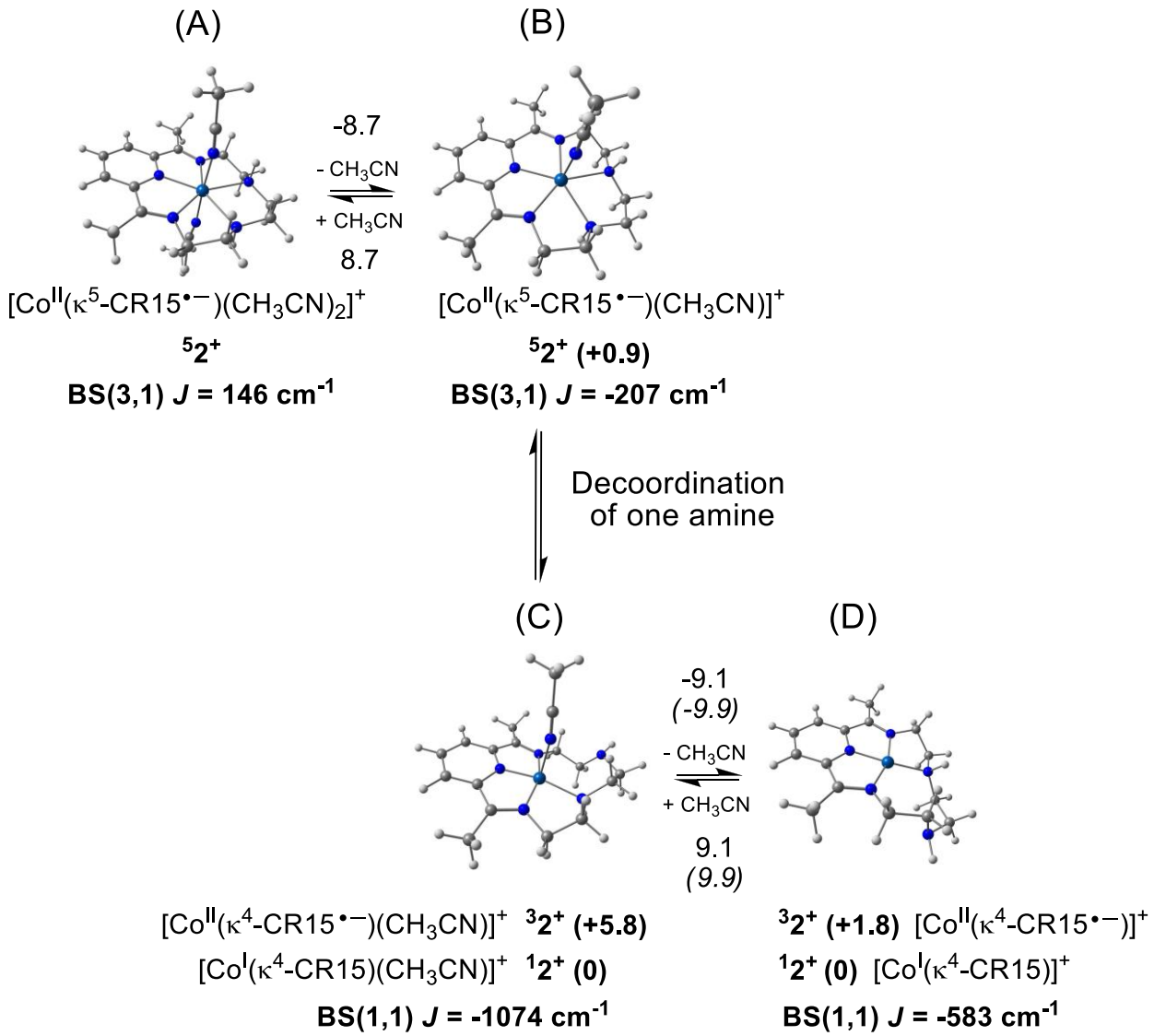


**Figure 5**. Geometry optimized structures for the quintet $^{5}\mathbf{2}^{+}$, triplet $^{3}\mathbf{2}^{+}$ and closed-shell singlet $^{1}\mathbf{2}^{+}$. The number under the arrow indicate the change in Gibbs energy $\Delta G_{binding}$ associated with the binding of one acetonitrile molecule (solid text high spin states, italic text low spin states). The relative energy of the possible spin states is indicated when two spin states can account for related geometries (A, B, C or D). A corresponds to the seven-coordinate, B the six-coordinate, C the square pyramidal and D the four-coordinate complexes. The magnetic coupling was calculated by using the Yamaguchi formula. The energies and $\Delta G_{binding}$ were calculated at the TPSSh/TZVP/COSMO level of theory. They are given in kcal/mol.

We next investigated the relative stability of the adducts formed with two (**A**), one (**B** and **C**) or no (**D**) axially bound acetonitrile molecule (Figure 5).[19b] In the gas phase the seven-coordinate complex **A** is favored over the monoadducts **B** and **C**, which are themselves more stable than the four-coordinate species **D**. In acetonitrile the four-coordinate complex **D** is the most stable structure. The low stability of the seven-coordinate complex when the solvent is considered is

consistent with the strong spectral homologies between $\mathbf{2}^+$ and $\mathbf{1}^+$, which suggest closely related structures and spin states. Accordingly, the $\Delta G_{binding}$ is found to be within the range of that calculated for $\mathbf{1}^+$ at the same level of theory.[34]

An energetic analysis was next undertaken. For both **C** and **D**, the BP86 and TPSSh functionals predict the Co(I) complex to be the most stable form. The triplet-singlet gap has been calculated at 9.0 and 5.8 kcal/mol for **C** with the BP86 and TPSSh functionals, respectively. For **D** it is 11.9 and 1.8 kcal/mol with the same functionals, respectively. When using the B3LYP functional the trend is reversed and the triplets become the most stable forms. With this functional the triplet-singlet gap is 4.6 and 2.8 kcal/mol for the square pyramidal **C** and four-coordinate **D** complexes, respectively. This result reflects the tendency of this hybrid functional, which contains 20% of Hartree Fock (HF) exchange, to favor high spin state, in contrast with the pure GGA functional BP86 and TPSSh functional (10 % of HF exchange). It is worth noting that the triplet-singlet gaps predicted for $\mathbf{2}^+$ (**C** and **D**) are similar than to those calculated at the same level of theory for $\mathbf{1}^+$ under similar geometry,[9b] within the uncertainty of the calculation. This points to a negligible influence of the lengthening of the alkylamine linker on the electronic structure in this family of cobalt complexes. We alternatively examined the reliability of broken symmetry solutions. For **C** and **D** the BS(1,1) state is systematically lower in energy than the triplet whatever the hybrid functional, consistent with antiferromagnetic interaction between the low spin Co(II) ion and a ligand radical (Figure 5). In other terms, in spite of the radical nature of the complex, it is predicted to exhibit a diamagnetic ground spin state.[35]

Finally, we computed the electronic spectra of the above species by TD-DFT (see Supporting Information). The most reasonable agreement with the experimental spectrum was obtained for the square pyramidal Co(I) complex **C** and the antiferromagnetically exchange-coupled four-coordinate radical species **D**. In the first case the lowest energy excitation is predicted at $\lambda_{calc}$ = 676 nm ($f_{osc}$ = 0.0353), which perfectly matches the experimental band centered at 698 nm (Figure 4). As depicted in Figure 6 it corresponds to a metal-to-ligand charge transfer. The energy of the NIR band is slightly underestimated in the case of **D**, as it is calculated at 815 nm ($f_{osc}$ = 0.0217). Hence, TD-DFT calculations strongly argue for an ($S$ = 0) spin state and a low-coordinate metal environment.

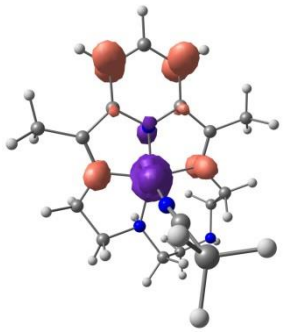

**Figure 6**. Plot of the TD-DFT difference density for the electronic excitation calculated at 676 nm ($f_{osc}$ = 0.0353) for the square pyramidal $^{1}$**2**$^{+}$. Red: positive value; Purple: Negative value. TPSSh/TZVP/COSMO calculation.

In conclusion, the above calculations consistently predict a diamagnetic ground spin state for **2**$^{+}$, in agreement with NMR measurements (Figure S2). They suggest a square-pyramidal Co(I) formulation of **2**$^{+}$, namely **C**, although the BS(1,1) four-coordinated species **D** remains a reliable alternative. As such, they confirm the homology both in terms of geometry and electronic structure between **2**$^{+}$ and the previously reported **1**$^{+}$ in similar media[9b] and show that the hybrid functional TPSSh is particularly useful for describing these families of complexes.[36]

**Electrochemical Properties of 2 in Acetonitrile in presence of Acids and in Water.** The electrochemical behavior of **2** has been investigated in acidic conditions in organic and aqueous solutions and compared to that of **1**.[9a, 37] In early works, we[9a] and others[37] have investigated the electrocatalytic behavior of **1** in $CH_3CN$ in the presence of *p*-cyanoanilium tetrafluoroborate (p$K_a$ = 7.6), tosic acid (p$K_a$ = 8.3) or trifluoroacetic acid (12.7).[38] With such relatively strong acids, a catalytic wave develops at potentials very close to the "Co(II)/Co(I)" wave of **1** ($E_{1/2}$ = -0.85 V *vs* $Ag/AgNO_3$), consistent with hydrogen evolution from protonation of the electrochemically generated "Co(I)" species.[9a, 37a] However it is not appropriate to investigate the electrocatalytic behavior of **2** in $CH_3CN$ in presence of such acids since their direct reduction at a glassy carbon electrode (onset potential at ~ -1.0 − -1.1V *vs* $Ag/AgNO_3$)[9a, 20j, 31, 39] are too close to the potential of the "Co(II)/Co(I)" wave of **2** ($E_{pc}$ = -1.32 V). We thus tested as a weaker acid, acetic acid (AcOH) (p$K_a$ = 22.3 in $CH_3CN$). The direct reduction of this acid at a glassy carbon electrode, characterized by a well-defined peak shape at $E_{pc}$ = -2.09 V (Figures 7A and S4), occurs this time at a potential close to that of the "Co(I)/Co(0)" wave of **2** ($E_{1/2}$ = -1.87 V). The addition of 1 mol equiv of AcOH (1 mM) to a 1 mM solution of **2** in $CH_3CN$ leads to the appearance of a new peak

at a slightly more positive potential than the "Co(I)/Co(0)" wave ($Ep_c$ = -1.81 V, onset potential ~ -1.60 V)) (Figures 7). The intensity of this catalytic wave increases progressively upon increasing the concentration of acid, while its onset potential shifts progressively towards more positive values (up to ~ -1.40 V at 30 mM AcOH, $Ep_c$ = -1.70 V) approaching the potential of the couple Co(II)/Co(I). No such catalytic wave is observed for **1** upon addition of similar amounts of acetic acid in a $CH_3CN$ solution (Figure S6). Instead, a continuous enhancement of the catalytic current is observed. This may indicate that, in the case of **2**, the amine released after reduction into the "Co(I)" state is protonated and acts as a proton relay fostering the $H_2$ evolution. This may be achieved through PCET reactions when the complex is further reduced to "Co(0)", for instance by promoting its protonation.[23a] However, photocatalytic experiments are performed in acidic water, and in this solvent, a catalytic proton reduction wave appeared at the potential of the "Co(II)/Co(I)" wave (see below). Thus, such experiments in $CH_3CN$ do not give any indication of the possible involvement of the free amine as proton relay when the complex is reduced *via* the "Co(I)" state since acetic acid is too weak to protonate the "Co(I)" center (the "Co(II)/Co(I)" reduction wave is not affected much by the presence of this acid (Figure S5)), and **2** needs to be further reduced to "Co(0)" to react with protons.

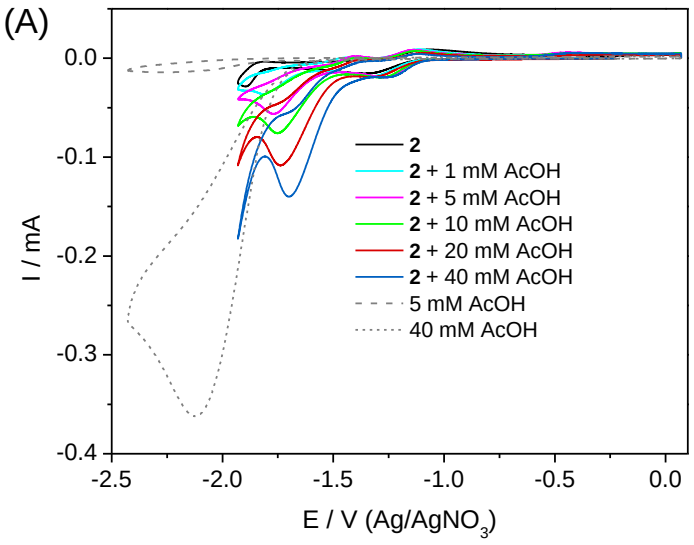

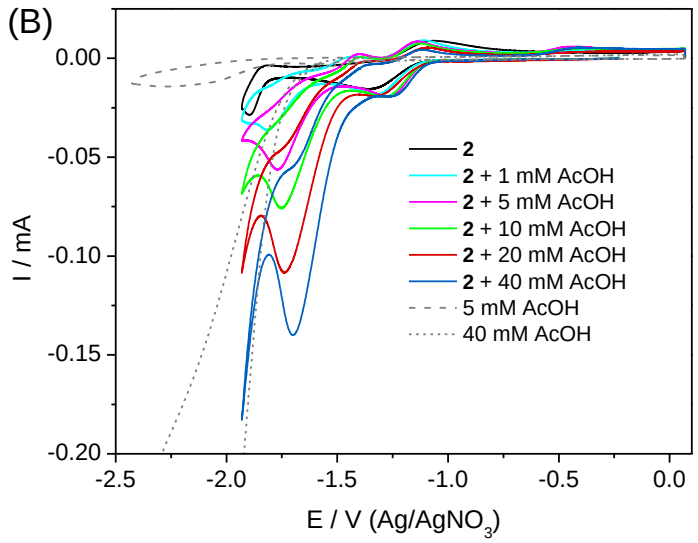


**Figure 7.** Cyclic voltammograms at a glassy carbon electrode ($\nu$ = 100 mV $s^{-1}$) in $CH_3CN$, 0.1 M $[Bu_4N]ClO_4$ of a 1 mM solution of $[Co(CR15)(H_2O)_2]Cl_2$ (**2**) and after addition of increasing amount of acetic acid (AcOH) (from 1 to 40 equiv) and of the acid without **2** (at 5 and 40 mM), scan range between 0.07 and -1.93 V (A), overscale (B).

In aqueous electrolyte, cyclic voltammograms were recorded both at pH 6.0 (0.1 M $NaNO_3$) and under the photocatalytic conditions, *i. e.* in aqueous buffered $HA^-/H_2A$ (1.1 M) solution at pH 4.5 (see below). At pH 6.0, the process formally assigned to "Co(II)/Co(I)" ($E_{1/2}$ = -1.01 V vs Ag/AgCl (3.0 M KCl)) is clearly observed, and appears as a quasi-reversible wave (Figure 8). This cyclic voltammogram is similar to that of **1** in aqueous solution except that the "Co(II)/Co(I)" wave of **1** is observed at a less negative potential ($Ep_c$ = -0.86 V *vs* Ag/AgCl for **1**),[9a] which is consistent with an additional coordinated amine in **2**. In aqueous buffered $HA^-/H_2A$ (1.1 M) solution at pH 4.5, the "Co(II)/Co(I)" wave of **2** becomes fully irreversible and a significant catalytic current is observed at this potential, fully consistent with an efficient $H_2$ evolution catalysis through the protonation of the Co(I) species at this pH. Assuming that the release of the amine occurs upon the reduction process, the fact that there is no shift toward more positive potential compared to the Co(II)/Co(I) wave by decreasing the pH from 6 to 4.5, seems however indicates that this amine does not play a pivotal role as a proton relay.[23c]

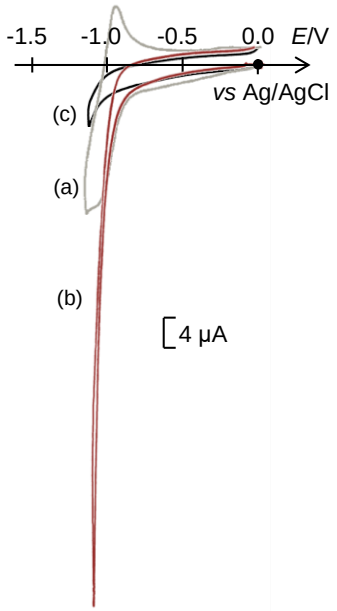


**Figure 8.** Cyclic voltammograms at a glassy carbon electrode ($\nu$ = 100 mV $s^{-1}$) of deaerated aqueous solutions of (a) 1 mM of **2** in presence of 0.1 M $NaNO_3$ at pH 6.0, (b) 1 mM of **2** in presence of $NaHA/H_2A$ (1.1 M) at pH 4.5, (c) $NaHA/H_2A$ (1.1 M) at pH 4.5 without catalyst. Potentials referenced to Ag/AgCl (3.0 M KCl) can be converted to SCE by subtracting 32 mV.

Anyway, in our photocatalytic conditions at pH 4.5, the reduced photosensitizer (denoted **Ru**$^{-}$), generated by reductive quenching of the excited state **Ru*** by $HA^-$ (see below) is an enough strong reductant (-1.47 V vs Ag/AgCl), to ensure the reduction of **2** into Co(I) and thus the catalysis.

**Photocatalytic Hydrogen Production.** The activity of **2** for the photo-induced hydrogen production was investigated with **Ru** as photosensitizer and ascorbate as sacrificial electron donor. Similarly to our previous experiments with **1**,[9a, 9b] the photocatalytic experiments were performed in deaerated fully aqueous solutions (5 mL) at 298 K under visible light irradiation (400-700 nm) with various PS and Cat concentrations in presence of the $HA^-/H_2A$ couple (total amount $[HA^-]$ and $[H_2A]$ of 1.1 M). The pH value has been adjusted by varying the relative concentrations of $HA^-$ and $H_2A$.[11a] The photogenerated $H_2$ was quantified in real time by gas chromatography, allowing the calculation of the TON and TOF values per molecule of catalyst.[9a] Table S4 summarizes the photocatalytic activities of all systems studied. All experiments were repeated at least three times and reproducible values within 5 % were obtained except for experiments conducted with the lowest catalyst concentration (1 µM) where the error margin reaches 15%. The

pH dependence of the photocatalytic activity of **Ru**/**2**/$HA^-$/$H_2A$ was evaluated with 500 µM **Ru**, 100 µM **2**, and a total concentration of 1.1 M $HA^-$/$H_2A$ (Figures 9 and S11). The highest performances were obtained at pH 4.5, while in similar experimental conditions, **1** exhibits its maximal catalytic activity at pH 4.0.[9a, 9b] In the case of **2**, it can be noticed that if initial TOF values are similar at pH 4.5 and 4.0, the stability of the photocatalytic system is higher at pH 4.5, resulting in significantly higher TON values after 21 h, *i. e.* 457 at pH 4.5 *vs* 342 at pH 4.0 (Figure 9). At higher pH, the stability of the photocatalytic system increases (at pH 6.0, the $H_2$ production is quasi-linear over 22 hours), but the TOFs decrease. Indeed, if the lower concentration in protons probably limits the decomposition of both photosensitizer and catalyst,[2, 11] the "Co(I)" species is less prone to react with protons.

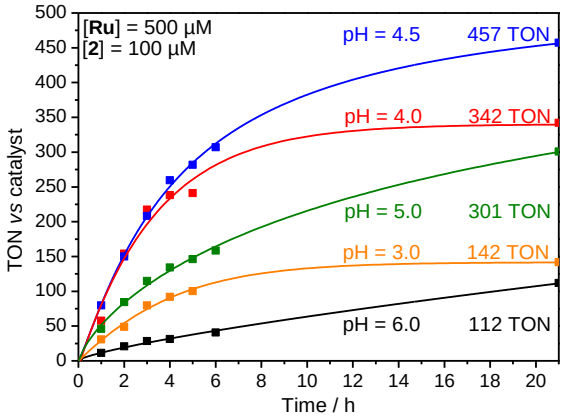


**Figure 9.** Photocatalytic hydrogen production (TON) as a function of time from a deaerated aqueous solution (5 mL) of NaHA/$H_2A$ (1.1 M), **Ru** (500 µM) and **2** (100 µM) under 400 – 700 nm irradiation at different pH; the pH of the solution is adjusted by the NaHA/$H_2A$ ratio ([NaHA]+[$H_2A$] = 1.1 M).

The photocatalytic activity of **2** was thus further evaluated at pH 4.5. Addition of Hg in the **Ru**/**2**/$HA^-$/$H_2A$ system induces no significant change in the photocatalytic activity, ruling out the involvement of cobalt metallic colloids into the $H_2$ production (Figure S12 and Supporting Information).[40] In addition, the absence of any induction period and the fact that no significant $H_2$ evolution was observed when **2** is substituted by a simple cobalt salt, such as $CoCl_2$•$6H_2O$, compared to $H_2$ produced from a **Ru**/$HA^-$/$H_2A$ solution (Table S4), are also clear indications that no Co(0) nanoparticules are formed during photocatalysis with **2**.[41]

The photocatalytic activity of the **Ru**/**2**/$HA^-$/$H_2A$ system was further investigated in various catalyst/photosensitizer ratios. At a relatively high concentration of catalyst (100 µM), with

increasing concentrations of **Ru** (100, 500 and 1 mM), the system produces efficiently $H_2$ with TON values of about 150, 457 and 603, respectively (Figures 10A and S13). With similar experimental catalyst/photosensitizer ratios but at a pH of 4.0, **1** exhibits higher performance with TON* values of 340, 820 and 1000 (Table S4).[9a] Control experiments with **2** in absence of **Ru** or $HA^-/H_2A$ produced no appreciable amount of hydrogen, while the production of a small quantity of $H_2$ was detected in solutions containing only **Ru** and $HA^-/H_2A$, in agreement with previous observations (Table S4, Figures S13).[9a, 9b, 11a] This production, due to the direct reduction of water by the reduced state of **Ru**, increases with **Ru** concentration (Figure S13B). It can be considered as negligible at catalyst concentrations of 100 μM because it represents less than 4% and is located within the margin of error (Figure S13A). However, as we will see below, at lower catalyst concentrations of 1 μM, this production of $H_2$ by **Ru** will represent up to 35% of the amount of $H_2$ produced by the **Ru**/**2**/$HA^-/H_2A$ system (Figure S14). Consequently, the values of TON and TOF were systematically corrected (denoted TON* and TOF*) by subtracting from the total volume of $H_2$ produced, the amount stemming from **Ru**/$HA^-/H_2A$ without catalyst, after 22 hours of irradiation (Table S4).

Then the dependence of the catalytic activity of **2** on lower catalyst concentrations (< 100 μM) has been explored. By maintaining the PS concentration constant at 500 μM, and decreasing the concentration of **2** up to 1 μM, the activity notably increases (Figures 10B, S14A and Table S4). As an example, when the concentration of **2** decreases from 50 μM to 1 μM, the TON* increases from 665 to 1660, corresponding to initial TOF* of about 170 to 5400. We did not further decrease the concentration of the catalyst since for concentrations lower than 1 μM, the amount of produced $H_2$ is close to the amount of the $H_2$ produced by the blank, **Ru** (500 μM) and $HA^-/H_2A$ (1.1 M) (Figure S13A). A similar dependence of $H_2$ production on the catalyst concentration was previously observed with similar photocatalytic systems employing rhodium and cobalt polypyridyl and porphyrin catalysts. [4c, 8c, 11a, 41-42] Such behavior is consistent with the presence of a large excess of PS compared to the catalyst, promoting the reduction of the latter. However, in such conditions, in agreement with previous observations,[9c] **Ru** is fully degraded after 22 h of irradiation (the catalyst acting as a quencher of the $\mathbf{Ru}^-$ species), while at least 80% of the initial **Ru** concentration is saved for a higher catalyst concentration of 100 μM after 22 h of irradiation (Figure S15). Interestingly, for **1** at pH 4.0, both TON and TOF significantly decrease upon decreasing the concentration of this catalyst below 50 μM, indicating that some deactivation

processes of the catalyst occur at low concentration at this pH.[9b] This is exemplified by the TON* of 715 and 590 which were previously measured for **1**[9b] at 10 and 5 µM, respectively, compared to 1086 and 1280 for **2** (Figures 10B, S14A and Table S4). Thus at concentrations of catalyst ≤ 50 µM and at pH 4.5, **2** appears to be a much more efficient $H_2$-evolving catalyst than **1** at pH 4.0. However, the experiments were not conducted at the same pH, pH 4.5 for **2** and pH 4.0 for **1**, and a higher pH can improve the stability of the system (catalyst and photosensitizer). Therefore, in order to ascertain that the observed differences in activities between **1** and **2** are not simply due to this pH difference, we also examined the catalytic activity of **1** at pH 4.5 in a concentration range of 100 – 1 µM (Figures 10C, S14B and Table S4). If at 100 and 50 µM, TON* (654 and 973, respectively) are lower than that at pH 4.0 (820 and 1130, respectively),[9a, 9b] TON continue to increase when decreasing the catalyst concentration. Indeed, TON* of 1204, 1322 and 1955 were measured at 10, 5 and 1 µM, respectively. This demonstrates that at a slightly higher pH of 4.5, **1** is less active but it is yet stabilized at low concentrations. Therefore, if we compare now the $H_2$-evolving activity of **1** and **2** at the same pH of 4.5, **1** follows the same behavior as that of **2**, namely a regular increase of TON upon decreasing the catalyst concentration (Figure 10B, C). In addition, at this pH, the $H_2$-evolving activity of **1** remains slightly higher than that of **2** whatever the concentration investigated (in the range 100 - 1 µM). Even if the initial TOF for low catalyst concentrations (≤ 10 µM) are slightly higher for **2** than for **1**, which could indicate that **2** is more reactive when its reduction is not limited by the amount of $\mathbf{Ru}^{-}$ species in solution, the photocatalytic system is less stable over time with **2** as catalyst, resulting in lower TON values for hydrogen production. Thus it appears that if the release of the amine upon reduction of **2** plays a role in promoting the $H_2$-evolving catalytic activity, other factors balance this effect. One of these factors may be the lower stability of **2** over **1** in the reduced "Co(I)" state in acidic aqueous solution induced by the release of the amine which renders the macrocycle more flexible thus promoting the decoordination of the metal.

Finally, we investigated the catalytic activities of **3-5** at 100 µM in presence of **Ru** at 500 µM at pH 4.5. As expected, these complexes are virtually inactive with a maximum of 6 TONs* for the zinc derivative (Figure S16 and Table S4).[9a] The reduced state of **Ru** ($E(Ru^{II/I})$ = -1.64 V vs $Ag/AgNO_3$,[43] (Table S4) is indeed not able to reduce efficiently these catalysts, for which the first reduction process (corresponding to a ligand centered process) is located at ~ -1.6 V.

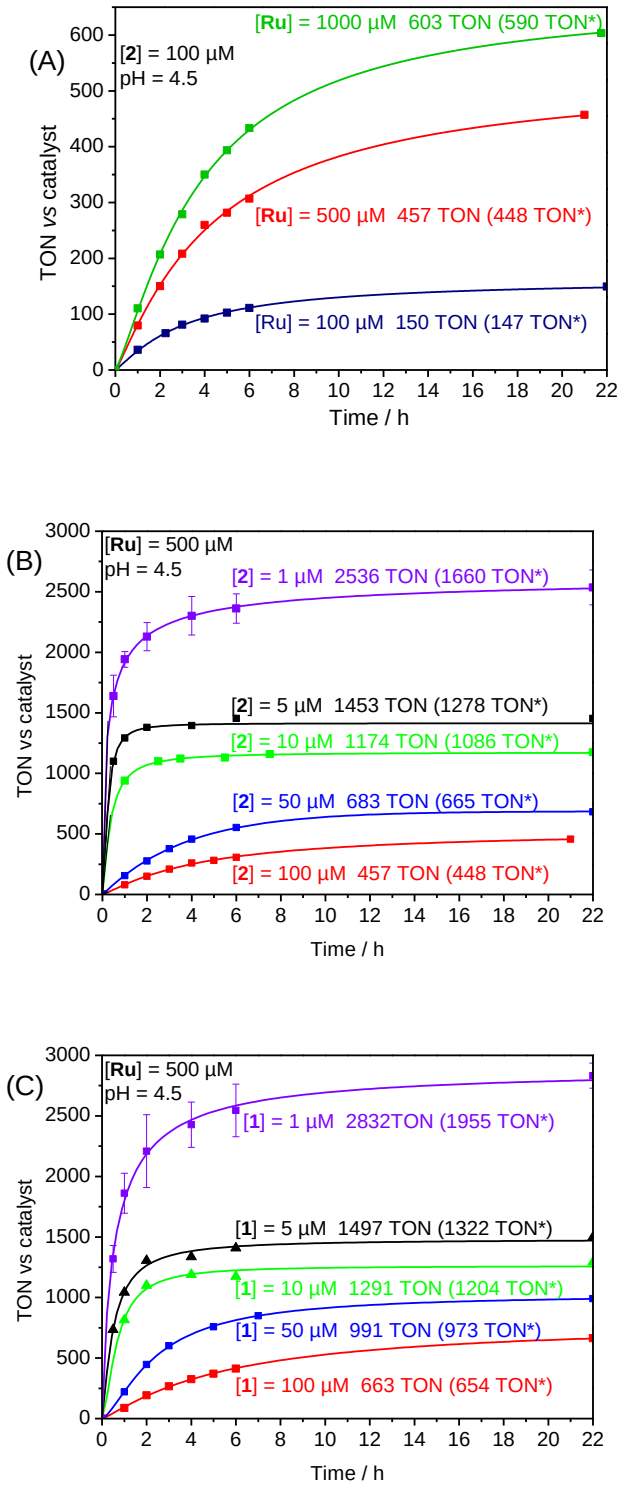


**Figure 10.** Photocatalytic hydrogen production (TON) as a function of time from a deaerated aqueous solution (5 mL) of NaHA/$H_2A$ (1.1 M) at pH 4.5 under 400 – 700 nm irradiation (A) in presence of **2** (100 µM) and **Ru** at various concentrations, (B) in presence of **Ru** (500 µM) and **2** at various concentrations and

(C) in presence of **Ru** (500 µM) and **1** at various concentrations. The error bars denote the standard deviation obtained for at least three experiments.

**Mechanistic Insight for the Ru/2/HA$^-$/H$_2$A System from Photophysical Measurements.** In such systems the initial photo-induced electron transfer process of photocatalytic cycle could be either a reductive quenching of the **Ru** excited state (denoted **Ru***) by HA$^-$ leading to the reduced state, [Ru$^{II}$(bpy)$_2$(bpy$^{\bullet-}$)]$^+$ (denoted **Ru**$^-$), or an oxidative quenching of **Ru*** by the catalyst leading to the Ru(III) state and to the reduced form of the catalyst.[2] Sutin[44] previously reported that the **Ru*** luminescence is quenched by HA$^-$ at pH 4.0 with a rate constant of $k_{q1}$= 2 x 10$^7$ M$^{-1}$ s$^{-1}$. We measured that the quenching rate of **Ru*** by **2** is $k_{q2}$ = 7 x 10$^7$ M$^{-1}$ s$^{-1}$ (Figure S18). Although this value is 3.5 times higher than that between **Ru*** and HA$^-$, the reductive quenching (with a pseudo-first order rate of 1.1 x 10$^7$ s$^{-1}$) dominates over oxidative one (7 x 10$^3$ s$^{-1}$ for 100 µM **2**), since the concentration of HA$^-$ (0.55 M) is much higher than that of **2** (from 1 to 100 µM). The reductive quenching is confirmed by a decrease of the H$_2$-evolving performance of the **Ru**/**2**/HA$^-$/H$_2$A photocatalytic system by decreasing the NaHA/H$_2$A concentration and keeping all the other parameters constant (Figure S17).

The occurrence of the reductive quenching is also supported by nanosecond laser flash photolysis experiments, which were performed by exciting at 455 nm deaerated aqueous solutions comprising **Ru** (100 µM), HA$^-$ (0.55 M), H$_2$A (0.55 M) in presence or absence of **2** (200 µM). The initial transient absorption spectra of **Ru**/HA$^-$/H$_2$A[9b, 11a, 44-45] and **Ru**/**2**/HA$^-$/H$_2$A systems (Figures 11 and S19) exhibit the three characteristic bands of **Ru*** at 370, 450 and 625 nm that correspond to the absorption of the radical anion located on bipyridine ligand, the ground state depopulation band of **Ru** and the emission of **Ru***, respectively. By monitoring these three bands, the time constant of **Ru*** extinction has been determined to be quasi identical with and without[9b] catalyst, respectively with 72 and 70 ns. These values are also relatively close to those obtained with catalysts **1** (64 ns) and [Co(N4Py)(H$_2$O)]$^{2+}$ (66 ns).[9b, 12] This confirms that, as with earlier systems, the reductive quenching of **Ru*** by HA$^-$ is the dominant mechanism. This reductive quenching leads to the formation of **Ru**$^-$ with a peculiar signature at 510 nm observed in the transient spectra[46] (Figures 11 and S19). In absence of **2**, we previously reported[9b] that **Ru**$^-$ decays is observed at 510 nm with two time constants of 11.6 µs (40 %) and 68.6 µs (60 %) *via* an intricate back electron transfer with the various oxidized forms of ascorbate such as the neutral radical HA$^{\bullet}$, the radical anion A$^{\bullet-}$ and the dehydroascorbic acid A.[2, 42h, 47] In presence of **2**, the decay of **Ru**$^-$ is faster and

monoexponential with a time constant of 2.8 µs, very close to that obtained previously in presence of **1** (2.9 µs) (Figure S19). From this value, and considering the concentration of **2** (200 µM), we estimated the bimolecular rate constant of the electron transfer from **Ru**$^{-}$ to **2** at 1.8 x $10^{9}$ $M^{-1}$ $s^{-1}$ (see ESI for calculation details). Similar kinetics have been found with the **Ru** photosensitizer and **1** (1.4 x $10^{9}$ $M^{-1}$ $s^{-1}$)[9b] or with other catalysts such as polypyridine cobalt [41, 42g, 42i, 42l, 47b] or rhodium[2, 11a, 45b, 45c] complexes.

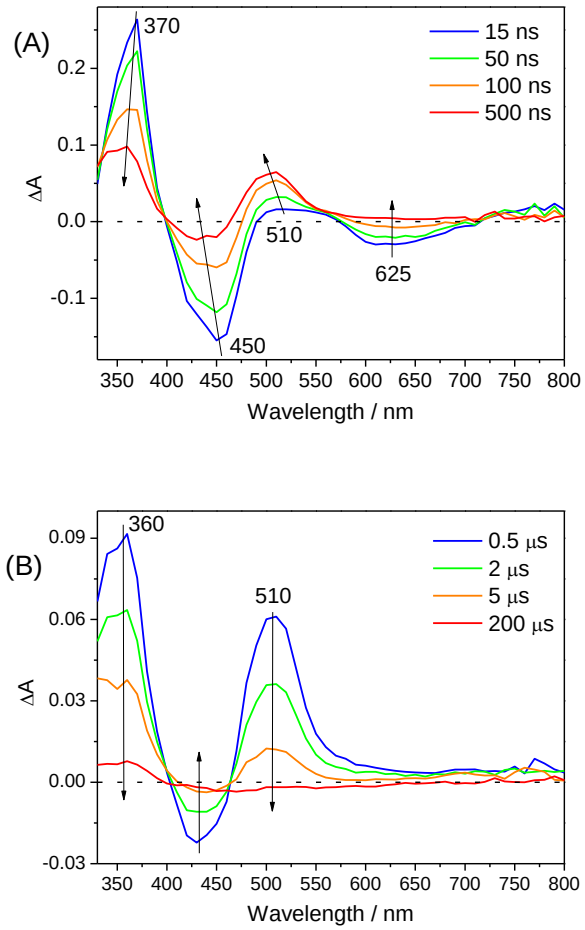


**Figure 11**. Transient absorption spectra after laser excitation (λ = 455 nm) of a deaerated aqueous solution containing **Ru** (100 µM), NaHA/$H_2A$ (1.1 M) at pH 4.5 in the presence of **2** (200 µM) (pathlength = 1 cm) within the time ranges 15–500 ns (A) 500 ns–200 µs (B).

Once the **Ru**$^{-}$ species is generated, it transfers its electron to the Co(II) catalyst, allowing the formation of the "Co(I)" species which is then protonated. Interestingly, additional features that can be ascribable to the "Co(I)" species (see above) are not observed concomitantly to the decay of the reduced **Ru**$^{-}$ species at 510 nm in the transient absorption spectra, while in similar

experimental conditions, the spectroscopic signature (large absorption band between 500 and 800 nm) of the "Co(I)" species of **1** has been observed.[46] Since the UV-visible signatures of the "Co(I)" species of **2** and **1** are very close (Figure 4), the absence of such signature for **2** suggests that this species reacts more rapidly with protons. The fact that the "Co(I)" species of **2** does not accumulate in solution could be in favor of a PCET process via the protonation of the extra amine with fast protonation of the "Co(I)" species, as previously inferred.[48]

## CONCLUSION

In this work, a cobalt complex with a pentaaza-macrocyclic Schiff base ligand (CR15) as well as its iron, manganese and zinc analogues were synthesized. All these complexes present a distorted pentagonal bipyramid geometry in which the metal center is heptacoordinated to two axial ligands ($H_2O$ or Cl) and five nitrogen atoms of the CR15 ligand in the plane. Electrochemical studies revealed a reduction potential for the Co(II)/Co(I) wave of about 400 mV more negative than that of the cobalt tetraazamacrocyclic (CR14) homologue **1** in acetonitrile, fully consistent with the coordination of an additional secondary amine of the CR15 ligand at the metal center. One of amine is released upon the one-electron reduction process of **2** into the formally "Co(I)" state as shown by the similarity of the visible absorption spectrum of this species in acetonitrile with that of the "Co(I)" species of **1** previously reported and could play the role of proton relay during the catalysis. This decoordination process upon reduction was also strongly supported by $^1$H NMR spectroscopy and TD-DFT calculations. These calculations also argue for a square-pyramidal closed-shell formulation of the one-electron reduced form of **2**, *i.e.* $[Co^{I}(\eta^4\text{-}CR15)(CH_3CN)]^+$, although the BS(1,1) four-coordinate species $[Co^{II}(\eta^4\text{-}CR15^{\bullet})]^+$ may be a reliable alternative.

Among the series of pentaaza-macrocyclic complexes, only the cobalt derivative (**2**) turned out to be very active for hydrogen production in water when associated to **Ru** and the $HA^-/H_2A$ couple. The activity is significant at pH 4.5, with 450 TON* at the highest catalyst concentration (100 μM) and reaches 1660 at the lowest concentration (1 μM). However, this activity remains slightly lower than that of **1** under similar experimental conditions, suggesting that if the amine released upon reduction of **2** plays a role in promoting the $H_2$-evolving catalytic activity, other factors balance this effect. Indeed, even if the initial TOF for lower catalyst concentrations (≤ 10 μM) are slightly

higher for **2** than for **1**, the photocatalytic system with **2** as catalyst appears to be less stable over time, resulting in lower TON values for hydrogen production. Interestingly, the absence of the typical signature of the "Co(I)" species for **2** in the nanosecond transient absorption spectra suggests that this species reacts more readily with protons. However, this pendant amine most probably makes the macrocycle more flexible and the catalyst less robust in the "Co(I)" state in acidic aqueous solution. This work thus emphasizes that adding a proton relay as a pendant group in close proximity to the metal center in order to keep intact the electronic properties of the metal center will be a more suitable strategy to improve the $H_2$-evolving catalytic performances of **1**. Works are in progress to introduce such substituents on the secondary amine of the tetraazamocrocyclic ligand.

## EXPERIMENTAL SECTION

**Synthesis of the complexes. [Co(CR15)($H_2O$)$_2$]$Cl_2$ (2).** This complex has been synthetized according to a procedure adapted from literature. Orange single crystals of [Co(CR15)($H_2O$)$_2$]$Cl_2$•4$H_2O$ (**2**•4$H_2O$) suitable for X-ray diffraction were obtained by dissolution of 20 mg of the orange powder of complex in water (3 mL) and slow evaporation of this solution under air. The structure is similar to that recently obtained by Wang.[27]

**[Fe(CR15)(X)$_2$](Y)$_2$ (X = Cl or X = $H_2O$ and Y = Cl) (3).** The synthesis was adapted from a literature procedure[29] and was performed under argon atmosphere in a glove box. $FeCl_2$•4$H_2O$ (500 mg, 2.51 mmol) was dissolved in a warmed mixture (50°C) of water (7.5 mL) and methanol (25 mL) leading to a red solution. 2,6-diacetylpyridine (410 mg, 2.51 mmol), solubilized in methanol (25 mL), and triethylenetetraamine (0.38 ml, 2.51 mmol) were added to the solution, which turned dark blue. After stirring at 70°C for 15 h, the dark blue solution was cooled at room temperature and the unreacted iron chloride (a red solid) was filtered off. The filtrate was evaporated to dryness affording a blue-green powder corresponding to **3**, which was collected by filtration and washed with diethyl ether (697 mg, yield, 52%). Anal. Calcd for $C_{15}H_{23}Cl_2FeN_5$•5.3$H_2O$•0.9$CH_3CN$ (532.56 g/mol): C, 37.89; H, 6.87; N, 15.52. Found: C, 37.8; H, 6.58; N, 15.6. ESI-MS *m/z* for $C_{15}H_{23}Cl_2FeN_5$ (M): 399.1 $[M]^+$, 363.2 $[M\text{-}H\text{-}Cl]^+$.

**[Mn(CR15)(CH$_3$CN)$_2$](PF$_6$)$_2$ (4)**. The synthesis was adapted from a literature procedure.[28] To a solution of Mn(OAc)$_2$·4H$_2$O (1 g, 4.08 mmol) in water (200 mL) was added a solution of 2,6-diacetylpyridine (666 mg, 4.08 mmol) in MeOH (200 mL). The resulting mixture was stirred at 55°C to ensure the complete dissolution of the 2,6-diacetylpyridine. 0.2 mL of acetic acid were added and the solution was stirred at 70°C for 30 minutes. Triethylenetetraamine (0.61 mL, 4.08 mmol) was then added and the resulting mixture was stirred at 70°C for 16h leading to an orange solution. After the addition of 2 equivalents of [NH$_4$]PF$_6$ (1.33 g, 8.16 mmol), the solution was concentrated under reduced pressure until the precipitation of bright orange microcrystals of compound **4** which were collected by filtration, washed with diethyl ether and dried under vacuum (760 mg). The filtrate was concentrated again under reduced pressure to give a second fraction of compound **4** which was also collected by filtration, washed with diethyl ether and dried under vacuum (430 mg). Overall yield 43.8 %. Anal. Calcd for C$_{15}$H$_{27}$F$_{12}$MnN$_5$O$_2$P$_2$•0.63H$_2$O (665.63 g/mol): C, 27.07; H, 4.28; N, 10.52. Found: C, 27.06; H, 4.30; N, 10.68. ESI-MS *m/z* for C$_{15}$H$_{27}$F$_{12}$MnN$_5$O$_2$P$_2$ (M): 363.2 [M-H-2PF$_6$]$^+$, 347.2 [M+H-H$_2$O-2PF$_6$]$^+$, 164.1 [M-2H$_2$O-2PF$_6$]$^{2+}$. Single crystals of [Mn(CR15)(CH$_3$CN)$_2$](PF$_6$)$_2$ were obtained by slow evaporation of isopropyl ether into an acetonitrile solution of **4**.

**{[Zn(CR15)(Cl)](PF$_6$)}$_n$ (5).** ZnCl$_2$ (573 mg, 4.2 mmol) was dissolved in a mixture of water (60 mL) and ethanol (60 mL) under stirring at 40°C. The temperature was increased to 50°C for 10 minutes and a solution of 2,6-diacetylpyridine (686 mg, 4.2 mmol) in ethanol (40 mL) was added, leading to a colorless solution. After 10 minutes of stirring at 70°C, triethylenetetraamine (0.63 mL, 4.2 mmol) was added dropwise. Acetic acid (0.17 mL) was then added and the resulting solution was stirred for 17h at 70°C. NaPF$_6$ was added in slight excess (756 mg, 4.5 mmol) and the mixture was concentrated under reduced pressure until precipitation of a bright white powder corresponding to the compound **5**, which was collected by filtration, washed with diethyl ether and dried under vacuum (1.22 g). The mother liquor was concentrated again until 10 mL leading to the precipitation of a new fraction of compound 5, which was collected by filtration, washed with diethyl ether and dried under vacuum (273 mg). Overall yield 64%. Anal. Calcd for C$_{15}$H$_{23}$ClF$_6$N$_5$PZn•2H$_2$O (555.21 g/mol): C, 32.45; H, 4.90; N, 12.61. Found: C, 32.45; H, 4.93; N, 12.73. ESI-MS *m/z* for C$_{15}$H$_{23}$ClF$_6$N$_5$PZn (M): Found: 372.2 [M-PF$_6$]$^+$, 168.6 [M-Cl-PF$_6$]$^{2+}$. $^1$H RMN (400 MHz, CD$_3$CN) δ = 8.31 (t, *J* = 8Hz, 1H, H$_{aro}$), 8.15 (d, *J* = 8Hz, 2H, H$_{aro}$), 3.87 (br s, 2H, CH$_2$), 3.54 (br s, 2H, CH$_2$), 3.10 (br s, 6H, CH$_2$), 2.63 (br s, 2H, NH), 2.47 (s, 6H, CH$_3$), 2.27

(br s, 2H, $CH_2$). Single crystals of {[Zn(CR15)(Cl)]($PF_6$)•$CH_3CN$}$_n$ were obtained by slow diffusion of isopropyl ether into an acetonitrile solution of the complex.

## ASSOCIATED CONTENT

**Supporting Information**.

This material is available free of charge on the ACS Publications website.

Materials and general experimental and theoretical details. Additional data for X-ray structure determination, electrochemistry, $^1$H NMR, DFT calculations, photocatalytic hydrogen production, photophysics, nanosecond transient absorption spectroscopy (Figures S1-S18 and Tables S1-S4).

CCDC 1893636 and CCDC 1893637 contain the supplementary crystallographic data for this paper. These data can be obtained free of charge via www.ccdc.cam.ac.uk/data_request/cif or by emailing data_request@ccdc.cam.ac.uk, or by contacting The Cambridge Crystallographic Data Centre, 12 Union Road, Cambridge CB2 1EZ, U.K.; fax: +44 1223 336033

## AUTHOR INFORMATION


### Corresponding Authors

*E-mail: fabrice.thomas@univ-grenoble-alpes.fr

jerome.fortage@univ-grenoble-alpes.fr

marie-noelle.collomb@univ-grenoble-alpes.fr

### ORCID

Carmen E. Castillo: 0000-0002-9549-559X
Fabrice Thomas: 0000-0002-6977-5192
Michel Sliwa: 0000-0002-5073-8180
Jérôme Chauvin: 0000-0001-5734-3969
Jérôme Fortage: 0000-0003-2673-0610
Marie-Noëlle Collomb: 0000-0002-6641-771X

### Present Adress

‖ Institute of Physics, ELI Beamlines, Academy of Sciences of the Czech Republic, Na Slovance 2, CZ-18221 Prague, Czech Republic

## Author Contributions

The manuscript was written through contributions of all authors. All authors have given approval to the final version of the manuscript.

## ACKNOWLEDGEMENTS

R.G.'s thanks the "Université Grenoble Alpes" for his PhD grant. This work has been partially supported by Labex ARCANE (ANR-11-LABX-0003-01) and CBH-EUR-GS (ANR-17-EURE-0003) for the project $H_2$Photocat including the C.E.C post-doctoral fellowship. This work was also supported by ICMG Chemistry Nanobio Platform (FR2067) and COST CM1202 program (PERSPECT $H_2O$). The authors thank the "Centre d' Expérimentation du Calcul Intensif en Chimie" (CECIC) for providing facilities for the DFT calculations and Pierre Girard for technical assistance. The Chevreul Institute (FR 2638), the Ministère de l'Enseignement Supérieur et de la Recherche, the Région Nord Pas de Calais and FEDER are acknowledged for financial support to M.S. and M.R.

## REFERENCES

1. Armaroli, N.; Balzani, V., The Hydrogen Issue. *ChemSusChem* **2011,** *4* (1), 21-36.
2. Stoll, T.; Castillo, C. E.; Kayanuma, M.; Sandroni, M.; Daniel, C.; Odobel, F.; Fortage, J.; Collomb, M.-N., Photo-Induced Redox Catalysis for Proton Reduction to Hydrogen with Homogeneous Molecular Systems using Rhodium-Based Catalysts. *Coord. Chem. Rev.* **2015,** *304–305*, 20-37.
3. Ozawa, H.; Yokoyama, Y.; Haga, M.; Sakai, K., Syntheses, characterization, and photo-hydrogen-evolving properties of tris(2,2 '-bipyridine) ruthenium(II) derivatives tethered to a cis-Pt(II)Cl-2 unit: insights into the structure-activity relationship. *Dalton Trans.* **2007,** (12), 1197-1206.
4. (a) Queyriaux, N.; Jane, R. T.; Massin, J.; Artero, V.; Chavarot-Kerlidou, M., Recent developments in hydrogen evolving molecular cobalt(II)–polypyridyl catalysts. *Coord. Chem. Rev.* **2015,** *304*, 3-19; (b) Han, Z.; Eisenberg, R., Fuel from Water: The Photochemical Generation of Hydrogen from Water. *Acc. Chem. Res.* **2014,** *47* (8), 2537-2544; (c) Zhao, X.; Wang, P.; Long, M., Electro- and Photocatalytic Hydrogen Production by Molecular Cobalt Complexes with Pentadentate Ligands. *Comments Inorg. Chem.* **2016**, 1-33; (d) Leung, C. F.; Cheng, S. C.; Yang, Y.; Xiang, J.; Yiu, S. M.; Ko, C. C.; Lau, T. C., Efficient photocatalytic water reduction by a cobalt(II) tripodal iminopyridine complex. *Catal. Sci. Technol.* **2018,** *8* (1), 307-313.
5. (a) Cao, W. N.; Wang, F.; Wang, H. Y.; Chen, B.; Feng, K.; Tung, C. H.; Wu, L. Z., Photocatalytic hydrogen production from a simple water-soluble FeFe -hydrogenase model

system. *Chem. Commun.* **2012,** *48* (65), 8081-8083; (b) Li, X. Q.; Wang, M.; Zheng, D. H.; Han, K.; Dong, J. F.; Sun, L. C., Photocatalytic $H_2$ Production in Aqueous Solution with Host-Guest Inclusions Formed by Insertion of an FeFe-Hydrogenase Mimic and an Organic Dye into Cyclodextrins. *Energy Environ. Sci.* **2012,** *5* (8), 8220-8224; (c) Orain, C.; Quentel, F.; Gloaguen, F., Photocatalytic Hydrogen Production Using Models of the Iron-Iron Hydrogenase Active Site Dispersed in Micellar Solution. *ChemSuschem* **2014,** *7* (2), 638-643.

6. Weingarten, A. S.; Kazantsev, R. V.; Palmer, L. C.; McClendon, M.; Koltonow, A. R.; Samuel, A. P. S.; Kiebala, D. J.; Wasielewski, M. R.; Stupp, S. I., Self-Assembling Hydrogel Scaffolds for Photocatalytic Hydrogen Production. *Nat. Chem.* **2014,** *6* (11), 964-970.

7. Eckenhoff, W. T., Molecular catalysts of Co, Ni, Fe, and Mo for hydrogen generation in artificial photosynthetic systems. *Coord. Chem. Rev.* **2018,** *373*, 295-316.

8. (a) Schnidrig, S.; Bachmann, C.; Müller, P.; Weder, N.; Spingler, B.; Joliat-Wick, E.; Mosberger, M.; Windisch, J.; Alberto, R.; Probst, B., Structure–Activity and Stability Relationships for Cobalt Polypyridyl-Based Hydrogen-Evolving Catalysts in Water. *ChemSusChem* **2017,** *10* (22), 4570-4580; (b) Joliat, E.; Schnidrig, S.; Probst, B.; Bachmann, C.; Spingler, B.; Baldridge, K. K.; von Rohr, F.; Schilling, A.; Alberto, R., Cobalt complexes of tetradentate, bipyridine-based macrocycles: their structures, properties and photocatalytic proton reduction. *Dalton Trans.* **2016,** *45* (4), 1737-1745; (c) Lucarini, F.; Pastore, M.; Vasylevskyi, S.; Varisco, M.; Solari, E.; Crochet, A.; Fromm, K. M.; Zobi, F.; Ruggi, A., Heptacoordinate $Co^{II}$ Complex as a New Architecture for Photochemical Hydrogen Production. *Chem. Eur. J.* **2017,** *23* (28), 6768-6771; (d) Lucarini, F.; Ruggi, A., Heptacoordinate Co(II) Catalyst for Light-driven Hydrogen Production in Fully Aqueous Medium. *CHIMIA International Journal for Chemistry* **2018,** *72* (4), 203-206; (e) Call, A.; Franco, F.; Kandoth, N.; Fernandez, S.; Gonzalez-Bejar, M.; Perez-Prieto, J.; Luis, J. M.; Lloret-Fillol, J., Understanding light-driven H2 evolution through the electronic tuning of aminopyridine cobalt complexes. *Chem. Sci.* **2018,** *9* (9), 2609-2619; (f) Queyriaux, N.; Giannoudis, E.; Windle, C. D.; Roy, S.; Pecaut, J.; Coutsolelos, A. G.; Artero, V.; Chavarot-Kerlidou, M., A noble metal-free photocatalytic system based on a novel cobalt tetrapyridyl catalyst for hydrogen production in fully aqueous medium. *Sustainable Energy & Fuels* **2018**; (g) Hogue, R. W.; Schott, O.; Hanan, G. S.; Brooker, S., A Smorgasbord of 17 Cobalt Complexes Active for Photocatalytic Hydrogen Evolution. *Chem. Eur. J. 24* (39), 9820-9832; (h) Lei, J.-M.; Luo, S.-P.; Zhan, S.-Z., A cobalt complex, a highly efficient catalyst for electro- and photochemical driven hydrogen generation in purely aqueous media. *Polyhedron* **2018,** *154*, 295-301; (i) Ahmad, E.; Majee, K.; Patel, J.; Das, B.; Padhi, S. K., Competent Electrocatalytic and Photocatalytic Proton Reduction by a Dechelated [Co(tpy)2]2+ Scaffold. *Eur. J. Inorg. Chem.* **2017,** *2017* (28), 3409-3418.

9. (a) Varma, S.; Castillo, C. E.; Stoll, T.; Fortage, J.; Blackman, A. G.; Molton, F.; Deronzier, A.; Collomb, M.-N., Efficient Photocatalytic Hydrogen Production in Water Using a Cobalt(III) Tetraaza-Macrocyclic Catalyst: Electrochemical Generation of the Low-Valent Co(I) Species and its Reactivity Toward Proton Reduction. *Phys. Chem. Chem. Phys.* **2013,** *15* (40), 17544-17552; (b) Gueret, R.; Castillo, C. E.; Rebarz, M.; Thomas, F.; Hargrove, A.-A.; Pécaut, J.; Sliwa, M.; Fortage, J.; Collomb, M.-N., Cobalt(III) Tetraaza-Macrocyclic Complexes as Efficient Catalyst for Photoinduced Hydrogen Production in Water: Theoretical Investigation of the Electronic Structure of the Reduced Species and Mechanistic Insight. *J. Photochem. Photobiol., B* **2015,** *152*, 82-94; (c) Gueret, R.; Poulard, L.; Oshinowo, M.; Chauvin, J.; Dahmane, M.; Dupeyre, G.; Lainé, P. P.; Fortage, J.; Collomb, M.-N., Challenging the $[Ru(bpy)_3]^{2+}$ Photosensitizer with a

Triazatriangulenium Robust Organic Dye for Visible-Light-Driven Hydrogen Production in Water. *ACS Catal.* **2018,** *8* (5), 3792-3802.
10. (a) Gimbert-Surinach, C.; Albero, J.; Stoll, T.; Fortage, J.; Collomb, M.-N.; Deronzier, A.; Palomares, E.; Llobet, A., Efficient and Limiting Reactions in Aqueous Light-Induced Hydrogen Evolution Systems using Molecular Catalysts and Quantum Dots. *J. Am. Chem. Soc.* **2014,** *136* (21), 7655-7661; (b) Sandroni, M.; Gueret, R.; Wegner, K. D.; Reiss, P.; Fortage, J.; Aldakov, D.; Collomb, M. N., Cadmium-free $CuInS_2$/ZnS quantum dots as efficient and robust photosensitizers in combination with a molecular catalyst for visible light-driven $H_2$ production in water. *Energy Environ. Sci.* **2018,** *11* (7), 1752-1761.
11. (a) Stoll, T.; Gennari, M.; Serrano, I.; Fortage, J.; Chauvin, J.; Odobel, F.; Rebarz, M.; Poizat, O.; Sliwa, M.; Deronzier, A.; Collomb, M.-N., $[Rh^{III}(dmbpy)_2Cl_2]^+$ as a Highly Efficient Catalyst for Visible-Light-Driven Hydrogen Production in Pure Water: Comparison with Other Rhodium Catalysts. *Chem. Eur. J.* **2013,** *19* (2), 782-792; (b) Kayanuma, M.; Stoll, T.; Daniel, C.; Odobel, F.; Fortage, J.; Deronzier, A.; Collomb, M.-N., A Computational Mechanistic Investigation of Hydrogen Production in Water Using the $[Rh^{III}(dmbpy)_2Cl_2]^+$/$[Ru^{II}(bpy)_3]^{2+}$/Ascorbic Acid Photocatalytic System. *Phys. Chem. Chem. Phys.* **2015,** *17* (16), 10497-10509.
12. Lo, W. K. C.; Castillo, C. E.; Gueret, R.; Fortage, J.; Rebarz, M.; Sliwa, M.; Thomas, F.; McAdam, C. J.; Jameson, G. B.; McMorran, D. A.; Crowley, J. D.; Collomb, M.-N.; Blackman, A. G., Synthesis, Characterization, and Photocatalytic $H_2$-Evolving Activity of a Family of $[Co(N_4Py)(X)]^{n+}$ Complexes in Aqueous Solution. *Inorg. Chem.* **2016,** *55* (9), 4564-4581.
13. Jacques, P. A.; Artero, V.; Pecaut, J.; Fontecave, M., Cobalt and nickel diimine-dioxime complexes as molecular electrocatalysts for hydrogen evolution with low overvoltages. *Proc. Natl. Acad. Sci. USA* **2009,** *106* (49), 20627-20632.
14. Roy, S.; Bacchi, M.; Berggren, G.; Artero, V., A Systematic Comparative Study of Hydrogen-Evolving Molecular Catalysts in Aqueous Solutions. *Chemsuschem* **2015,** *8* (21), 3632-3638.
15. (a) Baffert, C.; Artero, V.; Fontecave, M., Cobaloximes as functional models for hydrogenases. 2. proton electroreduction catalyzed by difluoroborylbis(dimethylglyoximato)cobalt(II) complexes in organic media. *Inorg. Chem.* **2007,** *46* (5), 1817-1824; (b) Du, P. W.; Schneider, J.; Luo, G. G.; Brennessel, W. W.; Eisenberg, R., Visible Light-Driven Hydrogen Production from Aqueous Protons Catalyzed by Molecular Cobaloxime Catalysts. *Inorg. Chem.* **2009,** *48* (11), 4952-4962.
16. (a) Zhang, W.; Hong, J.; Zheng, J.; Huang, Z.; Zhou, J. S.; Xu, R., Nickel-Thiolate Complex Assembled in One Step in Water for Solar $H_2$ production. *J. Am. Chem. Soc.* **2011,** *133* (51), 20680-20683; (b) Han, J. Y.; Zhang, W.; Zhou, T. H.; Wang, X.; Xu, R., Nickel-complexes with a mixed-donor ligand for photocatalytic hydrogen evolution from aqueous solutions under visible light. *Rsc Advances* **2012,** *2* (22), 8293-8296; (c) Han, Z. J.; Qiu, F.; Eisenberg, R.; Holland, P. L.; Krauss, T. D., Robust Photogeneration of H-2 in Water Using Semiconductor Nanocrystals and a Nickel Catalyst. *Science* **2012,** *338* (6112), 1321-1324.
17. Li, H.; Rauchfuss, T. B., Iron Carbonyl Sulfides, Formaldehyde, and Amines Condense To Give the Proposed Azadithiolate Cofactor of the Fe-Only Hydrogenases. *J. Am. Chem. Soc.* **2002,** *124* (5), 726-727.
18. Yamauchi, K.; Masaoka, S.; Sakai, K., Evidence for Pt(II)-Based Molecular Catalysis in the Thermal Reduction of Water into Molecular Hydrogen. *J. Am. Chem. Soc.* **2009,** *131* (24), 8404-8406.

19. (a) Lacy, D. C.; McCrory, C. C. L.; Peters, J. C., Studies of Cobalt-Mediated Electrocatalytic $CO_2$ Reduction Using a Redox-Active Ligand. *Inorg. Chem.* **2014,** *53* (10), 4980-4988; (b) Zhang, M.; El-Roz, M.; Frei, H.; Mendoza-Cortes, J. L.; Head-Gordon, M.; Lacy, D. C.; Peters, J. C., Visible Light Sensitized $CO_2$ Activation by the Tetraaza $[Co^{II}N_4H(MeCN)]^{2+}$ Complex Investigated by FT-IR Spectroscopy and DFT Calculations. *J. Phys. Chem. C* **2015,** *119* (9), 4645-4654.
20. (a) Dempsey, J. L.; Brunschwig, B. S.; Winkler, J. R.; Gray, H. B., Hydrogen Evolution Catalyzed by Cobaloximes. *Acc. Chem. Res.* **2009,** *42* (12), 1995-2004; (b) Solis, B. H.; Hammes-Schiffer, S., Theoretical Analysis of Mechanistic Pathways for Hydrogen Evolution Catalyzed by Cobaloximes. *Inorg. Chem.* **2011,** *50* (21), 11252-11262; (c) Muckerman, J. T.; Fujita, E., Theoretical studies of the mechanism of catalytic hydrogen production by a cobaloxime. *Chem. Commun.* **2011,** *47* (46), 12456-12458; (d) Marinescu, S. C.; Winkler, J. R.; Gray, H. B., Molecular mechanisms of cobalt-catalyzed hydrogen evolution. *Proc. Natl. Acad. Sci. USA* **2012,** *109* (38), 15127-15131; (e) Solis, B. H.; Yu, Y.; Hammes-Schiffer, S., Effects of Ligand Modification and Protonation on Metal Oxime Hydrogen Evolution Electrocatalysts. *Inorg. Chem.* **2013,** *52* (12), 6994-6999; (f) Estes, D. P.; Grills, D. C.; Norton, J. R., The Reaction of Cobaloximes with Hydrogen: Products and Thermodynamics. *J. Am. Chem. Soc.* **2014,** *136* (50), 17362-17365; (g) Solis, B. H.; Hammes-Schiffer, S., Proton-Coupled Electron Transfer in Molecular Electrocatalysis: Theoretical Methods and Design Principles. *Inorg. Chem.* **2014,** *53* (13), 6427-6443; (h) Rountree, E. S.; Martin, D. J.; McCarthy, B. D.; Dempsey, J. L., Linear Free Energy Relationships in the Hydrogen Evolution Reaction: Kinetic Analysis of a Cobaloxime Catalyst. *ACS Catal.* **2016,** *6* (5), 3326-3335; (i) Kaeffer, N.; Chavarot-Kerlidou, M.; Artero, V., Hydrogen Evolution Catalyzed by Cobalt Diimine Dioxime Complexes. *Acc. Chem. Res.* **2015,** *48* (5), 1286-1295; (j) Elgrishi, N.; McCarthy, B. D.; Rountree, E. S.; Dempsey, J. L., Reaction Pathways of Hydrogen-Evolving Electrocatalysts: Electrochemical and Spectroscopic Studies of Proton-Coupled Electron Transfer Processes. *ACS Catal.* **2016,** *6* (6), 3644-3659; (k) Lacy, D. C.; Roberts, G. M.; Peters, J. C., The Cobalt Hydride that Never Was: Revisiting Schrauzer's "Hydridocobaloxime". *J. Am. Chem. Soc.* **2015,** *137* (14), 4860-4864; (l) Lewandowska-Andralojc, A.; Baine, T.; Zhao, X.; Muckerman, J. T.; Fujita, E.; Polyansky, D. E., Mechanistic Studies of Hydrogen Evolution in Aqueous Solution Catalyzed by a Tertpyridine-Amine Cobalt Complex. *Inorg. Chem.* **2015,** *54* (9), 4310-4321; (m) Li, G.; Han, A.; Pulling, M. E.; Estes, D. P.; Norton, J. R., Evidence for Formation of a Co-H Bond from $(H_2O)_2Co(dmgBF_2)_2$ under $H_2$: Application to Radical Cyclizations. *J. Am. Chem. Soc.* **2012,** *134* (36), 14662-14665; (n) Mandal, S.; Shikano, S.; Yamada, Y.; Lee, Y.-M.; Nam, W.; Llobet, A.; Fukuzumi, S., Protonation Equilibrium and Hydrogen Production by a Dinuclear Cobalt-Hydride Complex Reduced by Cobaltocene with Trifluoroacetic Acid. *J. Am. Chem. Soc.* **2013,** *135* (41), 15294-15297.
21. (a) Solis, B. H.; Maher, A. G.; Dogutan, D. K.; Nocera, D. G.; Hammes-Schiffer, S., Nickel phlorin intermediate formed by proton-coupled electron transfer in hydrogen evolution mechanism. *Proc. Natl. Acad. Sci.* **2016,** *113* (3), 485-492; (b) Henke, W. C.; Lionetti, D.; Moore, W. N. G.; Hopkins, J. A.; Day, V. W.; Blakemore, J. D., Ligand Substituents Govern the Efficiency and Mechanistic Path of Hydrogen Production with Cp*Rh Catalysts. *Chemsuschem* **2017,** *10* (22), 4589-4598; (c) Quintana, L. M. A.; Johnson, S. I.; Corona, S. L.; Villatoro, W.; Goddard, W. A.; Takase, M. K.; VanderVelde, D. G.; Winkler, J. R.; Gray, H. B.; Blakemore, J. D., Proton-hydride tautomerism in hydrogen evolution catalysis. *Proc. Natl. Acad. Sci. USA* **2016,** *113* (23), 6409-6414; (d) Chalkley, M. J.; Del Castillo, T. J.; Matson, B. D.; Roddy, J. P.; Peters, J. C., Catalytic

N2-to-NH3 Conversion by Fe at Lower Driving Force: A Proposed Role for Metallocene-Mediated PCET. *ACS Central Science* **2017,** *3* (3), 217-223.
22. Blackman, A. G., Cobalt: Inorganic and Coordination Chemistry. *Encyclopedia of Inorganic Chemistry, 2nd ed., (Ed.: R. B. King), Wiley* **2006**, p. 967-991.
23. (a) Lee, C. H.; Dogutan, D. K.; Nocera, D. G., Hydrogen Generation by Hangman Metalloporphyrins. *J. Am. Chem. Soc.* **2011,** *133* (23), 8775-8777; (b) Bediako, D. K.; Solis, B. H.; Dogutan, D. K.; Roubelakis, M. M.; Maher, A. G.; Lee, C. H.; Chambers, M. B.; Hammes-Schiffer, S.; Nocera, D. G., Role of pendant proton relays and proton-coupled electron transfer on the hydrogen evolution reaction by nickel hangman porphyrins. *Proc. Natl. Acad. Sci.* **2014,** *111* (42), 15001-15006; (c) Willkomm, J.; Muresan, N. M.; Reisner, E., Enhancing H2 evolution performance of an immobilised cobalt catalyst by rational ligand design. *Chem. Sci.* **2015,** *6* (5), 2727-2736; (d) Stewart, M. P.; Ho, M.-H.; Wiese, S.; Lindstrom, M. L.; Thogerson, C. E.; Raugei, S.; Bullock, R. M.; Helm, M. L., High Catalytic Rates for Hydrogen Production Using Nickel Electrocatalysts with Seven-Membered Cyclic Diphosphine Ligands Containing One Pendant Amine. *J. Am. Chem. Soc.* **2013,** *135* (16), 6033-6046; (e) Bourrez, M.; Steinmetz, R.; Gloaguen, F., Mechanistic Insights into the Catalysis of Electrochemical Proton Reduction by a Diiron Azadithiolate Complex. *Inorg. Chem.* **2014,** *53* (19), 10667-10673; (f) Basu, D.; Mazumder, S.; Shi, X.; Staples, R. J.; Schlegel, H. B.; Verani, C. N., Distinct Proton and Water Reduction Behavior with a Cobalt(III) Electrocatalyst Based on Pentadentate Oximes. *Angew. Chem. Int. Ed.* **2015,** *54* (24), 7139-7143; (g) Koshiba, K.; Yamauchi, K.; Sakai, K., A Nickel Dithiolate Water Reduction Catalyst Providing Ligand-Based Proton-Coupled Electron-Transfer Pathways. *Angew. Chem., Int. Ed. Engl.* **2017,** *56* (15), 4247-4251.
24. Chen, L.; Guo, Z.; Wei, X.-G.; Gallenkamp, C.; Bonin, J.; Anxolabehere-Mallart, E.; Lau, K.-C.; Lau, T.-C.; Robert, M., Molecular Catalysis of the Electrochemical and Photochemical Reduction of $CO_2$ with Earth-Abundant Metal Complexes. Selective Production of CO vs HCOOH by Switching of the Metal Center. *J. Am. Chem. Soc.* **2015,** *137* (34), 10918-10921.
25. (a) Curry, J. D.; Busch, D. H., The Reactions of Coordinated Ligands. VII. Metal Ion Control in the Synthesis of Chelate Compounds Containing Pentadentate and Sexadentate Macrocyclic Ligands. *J. Am. Chem. Soc.* **1964,** *86* (4), 592-594; (b) Long, K. M.; Busch, D. H., *J. Coord. Chem.* **1974,** *4*, 113-123.
26. Rezaeivala, M.; Keypour, H., Schiff base and non-Schiff base macrocyclic ligands and complexes incorporating the pyridine moiety – The first 50 years. *Coord. Chem. Rev.* **2014,** *280*, 203-253.
27. Huang, X.-C.; Zhou, C.; Shao, D.; Wang, X.-Y., Field-Induced Slow Magnetic Relaxation in Cobalt(II) Compounds with Pentagonal Bipyramid Geometry. *Inorg. Chem.* **2014,** *53* (24), 12671-12673.
28. Begum, F.; Khan, M. S.; Haider, S. Z.; Malik, K. M. A.; Khan, F. K., Synthesis, characterization and properties of some macrocyclic compounds of manganese (II), magnesium (II), cadmium (II) and cobalt (II). *J. Bangladesh Acad. Sci.* **1991,** *15* (2), 185-191.
29. Venkatakrishnan, T. S.; Sahoo, S.; Bréfuel, N.; Duhayon, C.; Paulsen, C.; Barra, A.-L.; Ramasesha, S.; Sutter, J.-P., Enhanced Ion Anisotropy by Nonconventional Coordination Geometry: Single-Chain Magnet Behavior for a $[\{Fe^{II}L\}_2\{Nb^{IV}(CN)_8\}]$ Helical Chain Compound Designed with Heptacoordinate $Fe^{II}$. *J. Am. Chem. Soc.* **2010,** *132* (17), 6047-6056.
30. Ghosh, M.; Weyhermuller, T.; Wieghardt, K., Electronic structure of the members of the electron transfer series $[NiL]^z$ (z=3+, 2+, 1+, 0) and $[NiL(X)]^n$ (X = Cl, CO, $P(OCH_3)_3$) species

containing a tetradentate, redox-noninnocent, Schiff base macrocyclic ligand L: an experimental and density functional theoretical study. *Dalton Trans.* **2010,** *39* (8), 1996-2007.
31. Castillo, C. E.; Stoll, T.; Sandroni, M.; Gueret, R.; Fortage, J.; Kayanuma, M.; Daniel, C.; Odobel, F.; Deronzier, A.; Collomb, M.-N., Electrochemical Generation and Spectroscopic Characterization of the Key Rhodium(III) Hydride Intermediates of Rhodium Poly(bipyridyl) $H_2$-Evolving Catalysts. *Inorg. Chem.* **2018,** *57* (17), 11225-11239.
32. (a) Darmon, J. M.; Stieber, S. C. E.; Sylvester, K. T.; Fernández, I.; Lobkovsky, E.; Semproni, S. P.; Bill, E.; Wieghardt, K.; DeBeer, S.; Chirik, P. J., Oxidative Addition of Carbon–Carbon Bonds with a Redox-Active Bis(imino)pyridine Iron Complex. *J. Am. Chem. Soc.* **2012,** *134* (41), 17125-17137; (b) Tondreau, A. M.; Stieber, S. C. E.; Milsmann, C.; Lobkovsky, E.; Weyhermüller, T.; Semproni, S. P.; Chirik, P. J., Oxidation and Reduction of Bis(imino)pyridine Iron Dinitrogen Complexes: Evidence for Formation of a Chelate Trianion. *Inorg. Chem.* **2013,** *52* (2), 635-646.
33. A hexacoordinated triplet could be hardly converged, wherein the metal ion lies in a pentagonal pyramidal geometry. This spin state shows significant spin contamination whatever the functional used. The predicted Co-N bond distances, while not accurately predicted due to spin contamination, are comparable to $\mathbf{5}^{2+}$. We take this as further evidence for a broken-symmetry character of this triplet.
34. For the square pyramidal to square planar conversion in the case of $\mathbf{1}^{+}$ the DG are -8.3 kcal/mol (triplet) and -5.6 kcal/mol (singlet) (TPSSh/TZVP/COSMO).
35. For B the BS(3,1) state is lower in energy than the quintet, showing that the magnetic coupling between the high spin Co(II) and the ligand-radical is again antiferromagnetic, whereas calculations predict a ferromagnetic interaction in the seven-coordinate complex A.
36. Jensen, K. P., Bioinorganic Chemistry Modeled with the TPSSh Density Functional. *Inorg. Chem.* **2008,** *47* (22), 10357-10365.
37. (a) Leung, C. F.; Chen, Y. Z.; Yu, H. Q.; Yiu, S. M.; Ko, C. C.; Lau, T. C., Electro- and photocatalytic hydrogen generation in acetonitrile and aqueous solutions by a cobalt macrocyclic Schiff-base complex. *Int. J. Hydrogen Energy* **2011,** *36* (18), 11640-11645; (b) Lee, C. H.; Villágran, D.; Cook, T. R.; Peters, J. C.; Nocera, D. G., Pacman and Hangman Metal Tetraazamacrocycles. *ChemSusChem* **2013,** *6* (8), 1541-1544.
38. Fourmond, V.; Jacques, P. A.; Fontecave, M.; Artero, V., $H_2$ Evolution and Molecular Electrocatalysts: Determination of Overpotentials and Effect of Homoconjugation. *Inorg. Chem.* **2010,** *49* (22), 10338-10347.
39. McCarthy, B. D.; Martin, D. J.; Rountree, E. S.; Ullman, A. C.; Dempsey, J. L., Electrochemical Reduction of Bronsted Acids by Glassy Carbon in Acetonitrile-Implications for Electrocatalytic Hydrogen Evolution. *Inorg. Chem.* **2014,** *53* (16), 8350-8361.
40. (a) Amouyal, E.; Koffi, P., Photochemical Production of Hydrogen from Water *J. Photochem.* **1985,** *29* (1-2), 227-242; (b) Anton, D. R.; Crabtree, R. H., Dibenzo[A,E]Cyclooctatetraene in a Proposed Test for Heterogeneity in Catalysts Formed From Soluble Platinum Group Metal-Complexes. *Organometallics* **1983,** *2* (7), 855-859; (c) Galan, B. R.; Reback, M. L.; Jain, A.; Appel, A. M.; Shaw, W. J., Electrocatalytic Oxidation of Formate with Nickel Diphosphine Dipeptide Complexes: Effect of Ligands Modified with Amino Acids. *Eur. J. Inorg. Chem.* **2013,** *2013* (30), 5366-5371.
41. Khnayzer, R. S.; Thoi, V. S.; Nippe, M.; King, A. E.; Jurss, J. W.; El Roz, K. A.; Long, J. R.; Chang, C. J.; Castellano, F. N., Towards a Comprehensive Understanding of Visible-Light

Photogeneration of Hydrogen from Water Using Cobalt(II) Polypyridyl Catalysts. *Energy Environ. Sci.* **2014,** *7* (4), 1477-1488.
42. (a) Singh, W. M.; Baine, T.; Kudo, S.; Tian, S.; Ma, X. A. N.; Zhou, H.; DeYonker, N. J.; Pham, T. C.; Bollinger, J. C.; Baker, D. L.; Yan, B.; Webster, C. E.; Zhao, X., Electrocatalytic and Photocatalytic Hydrogen Production in Aqueous Solution by a Molecular Cobalt Complex. *Angew. Chem. Int. Ed.* **2012,** *51*, 5941-5944; (b) Vennampalli, M.; Liang, G.; Katta, L.; Webster, C. E.; Zhao, X., Electronic Effects on a Mononuclear Co Complex with a Pentadentate Ligand for Catalytic $H_2$ Evolution. *Inorg. Chem.* **2014,** *53* (19), 10094-10100; (c) Guttentag, M.; Rodenberg, A.; Bachmann, C.; Senn, A.; Hamm, P.; Alberto, R., A Highly Stable Polypyridyl-Based Cobalt Catalyst for Homo- and Heterogeneous Photocatalytic Water Reduction. *Dalton Trans.* **2013,** *42* (2), 334-337; (d) Bachmann, C.; Guttentag, M.; Spingler, B.; Alberto, R., 3d Element Complexes of Pentadentate Bipyridine-Pyridine-Based Ligand Scaffolds: Structures and Photocatalytic Activities. *Inorg. Chem.* **2013,** *52* (10), 6055-6061; (e) Bachmann, C.; Probst, B.; Guttentag, M.; Alberto, R., Ascorbate as an Electron Relay Between an Irreversible Electron Donor and Ru(II) or Re(I) Photosensitizers. *Chem. Commun.* **2014,** *50* (51), 6737-6739; (f) Sun, Y. J.; Sun, J. W.; Long, J. R.; Yang, P. D.; Chang, C. J., Photocatalytic generation of hydrogen from water using a cobalt pentapyridine complex in combination with molecular and semiconductor nanowire photosensitizers. *Chem. Sci.* **2013,** *4* (1), 118-124; (g) Singh, W. M.; Mirmohades, M.; Jane, R. T.; White, T. A.; Hammarstrom, L.; Thapper, A.; Lomoth, R.; Ott, S., Voltammetric and Spectroscopic Characterization of Early Intermediates in the Co(II)-Polypyridyl-Catalyzed Reduction of Water. *Chem. Commun.* **2013,** *49* (77), 8638-8640; (h) Guttentag, M.; Rodenberg, A.; Kopelent, R.; Probst, B.; Buchwalder, C.; Brandstätter, M.; Hamm, P.; Alberto, R., Photocatalytic H2 Production with a Rhenium/Cobalt System in Water under Acidic Conditions. *Eur. J. Inorg. Chem.* **2012,** *2012* (1), 59-64; (i) Natali, M.; Luisa, A.; lengo, E.; Scandola, F., Efficient Photocatalytic Hydrogen Generation from Water by a Cationic Cobalt(II) Porphyrin. *Chem. Commun.* **2014,** *50* (15), 1842-1844; (j) Nippe, M.; Khnayzer, R. S.; Panetier, J. A.; Zee, D. Z.; Olaiya, B. S.; Head-Gordon, M.; Chang, C. J.; Castellano, F. N.; Long, J. R., Catalytic proton reduction with transition metal complexes of the redox-active ligand $bpy_2PYMe$. *Chem. Sci.* **2013,** *4* (10), 3934-3945; (k) Tong, L. P.; Zong, R. F.; Thummel, R. P., Visible Light-Driven Hydrogen Evolution from Water Catalyzed by A Molecular Cobalt Complex. *J. Am. Chem. Soc.* **2014,** *136* (13), 4881-4884; (l) Deponti, E.; Luisa, A.; Natali, M.; Iengo, E.; Scandola, F., Photoinduced Hydrogen Evolution by a Pentapyridine Cobalt Complex: Elucidating Some Mechanistic Aspects. *Dalton Trans.* **2014,** *43*, 16345-16353.
43. (a) Baffert, C.; Dumas, S.; Chauvin, J.; Leprêtre, J.-C.; Collomb, M.-N.; Deronzier, A., Photoinduced oxidation of $[Mn(L)_3]^{2+}$ and $[Mn_2O_2(L)_4]^{3+}$ (L = 2,2'-bipyridine and 4,4'-dimethyl-2,2'-bipyridine) with the $[Ru(bpy)_3]^{2+}$/-aryl diazonium salt system. *Phys. Chem. Chem. Phys.* **2005,** *7*, 202-210; (b) Collomb, M.-N.; Deronzier, A., Electro- and Photoinduced Formation and Transformation of Oxido-Bridged Multinuclear Mn Complexes. *Eur. J. Inorg. Chem.* **2009**, 2025-2046.
44. Creutz, C.; Sutin, N.; Brunschwig, B. S., Excited-State Photochemistry in the Tris(2,2'-Bipyridine)Ruthenium(II)-Sulfite System *J. Am. Chem. Soc.* **1979,** *101* (5), 1297-1298.
45. (a) Oishi, S., A Water-Soluble Wilkinsons Complex as Homogeneous Catalyst for the Photochemical Reduction of Water. *J. Mol. Catal.* **1987,** *39* (2), 225-232; (b) Fukuzumi, S.; Kobayashi, T.; Suenobu, T., Photocatalytic Production of Hydrogen by Disproportionation of One-Electron-Reduced Rhodium and Iridium–Ruthenium Complexes in Water. *Angew. Chem. Int. Ed.* **2011,** *50* (3), 728-731; (c) Stoll, T.; Gennari, M.; Fortage, J.; Castillo, C. E.; Rebarz, M.; Sliwa,

M.; Poizat, O.; Odobel, F.; Deronzier, A.; Collomb, M.-N., An Efficient $Ru^{II}$-$Rh^{III}$-$Ru^{II}$ Polypyridyl Photocatalyst for Visible-Light-Driven Hydrogen Production in Aqueous Solution. *Angew. Chem., Int. Ed. Engl.* **2014,** *53* (6), 1654-1658.
46. Mulazzani, Q. G.; Emmi, S.; Fuochi, P. G.; Hoffman, M. Z.; Venturi, M., On the nature of tris(2,2'-bipyridine)ruthenium(1+) ion in aqueous solution. *J. Am. Chem. Soc.* **1978,** *100* (3), 981-983.
47. (a) Krishnan, C. V.; Sutin, N., Homogeneous Catalysis of the Photo-Reduction of Water by Visible-Light. 2. Mediation by a Tris(2,2'-Bipyridine)Ruthenium(II)-Cobalt(II) Bipyridine System. *J. Am. Chem. Soc.* **1981,** *103* (8), 2141-2142; (b) Shan, B.; Baine, T.; Ma, X. A. N.; Zhao, X.; Schmehl, R. H., Mechanistic Details for Cobalt Catalyzed Photochemical Hydrogen Production in Aqueous Solution: Efficiencies of the Photochemical and Non-Photochemical Steps. *Inorg. Chem.* **2013,** *52* (9), 4853-4859.
48. Natali, M., Elucidating the Key Role of pH on Light-Driven Hydrogen Evolution by a Molecular Cobalt Catalyst. *ACS Catal.* **2017**, 1330-1339.

**TOC**

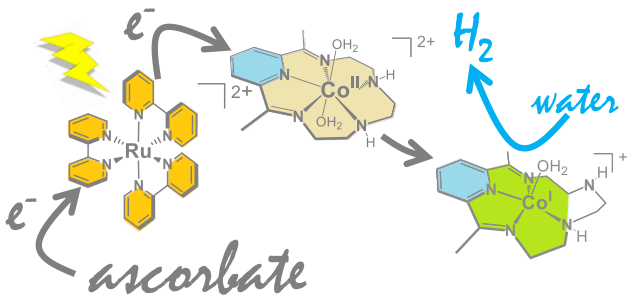


The cobalt(II) pentaza-macrocyclic Schiff Base complex is an efficient catalyst for $H_2$ production from water when used in a photocatalytic system with $[Ru(bpy)_3]^{2+}$ as the photosensitizer and ascorbate as the sacrificial electron donor. Electrochemical and spectroscopic investigations in $CH_3CN$ coupled to density functional theory (DFT) calculations evidenced a decoordination of one of the amine upon reduction of Co(II) to the low-valent "Co(I)" form. This unchelated amine of the CR15 ligand could potentially act as a proton relay promoting the $H_2$ production via proton-coupled-electron transfer (PCET) reactions.